XCR1$^+$ dendritic cells promote memory CD8$^+$ T cell recall upon secondary infections with *Listeria monocytogenes* or certain viruses

Yannick O. Alexandre,[1] Sonia Ghilas,[1] Cindy Sanchez,[1] Agnès Le Bon,[2] Karine Crozat,[1]* and Marc Dalod[1]*

[1]Centre d'Immunologie de Marseille-Luminy, Aix Marseille Université UM2, Institut National de la Santé et de la Recherche Médicale, U1104, Centre National de la Recherche Scientifique UMR7280, 13288 Marseille, France
[2]Institut Cochin, Institut National de la Santé et de la Recherche Médicale, U1016, Centre National de la Recherche Scientifique UMR8104, Université Paris Descartes, Sorbonne Paris Cité, 75014 Paris, France

Naive CD8$^+$ T cell priming during tumor development or many primary infections requires cross-presentation by XCR1$^+$ dendritic cells (DCs). Memory CD8$^+$ T lymphocytes (mCTLs) harbor a lower activation threshold as compared with naive cells. However, whether their recall responses depend on XCR1$^+$ DCs is unknown. By using a new mouse model allowing fluorescent tracking and conditional depletion of XCR1$^+$ DCs, we demonstrate a differential requirement of these cells for mCTL recall during secondary infections by different pathogens. XCR1$^+$ DCs were instrumental to promote this function upon secondary challenges with *Listeria monocytogenes*, vesicular stomatitis virus, or Vaccinia virus, but dispensable in the case of mouse cytomegalovirus. We deciphered how XCR1$^+$ DCs promote mCTL recall upon secondary infections with *Listeria*. By visualizing for the first time the in vivo choreography of XCR1$^+$ DCs, NK cells and mCTLs during secondary immune responses, and by neutralizing in vivo candidate molecules, we demonstrate that, very early after infection, mCTLs are activated, and attracted in a CXCR3-dependent manner, by NK cell–boosted, IL-12–, and CXCL9-producing XCR1$^+$ DCs. Hence, depending on the infectious agent, strong recall of mCTLs during secondary challenges can require cytokine- and chemokine-dependent cross-talk with XCR1$^+$ DCs and NK cells.

Conventional DCs constitute a rare and heterogeneous population of cells with unique antigen (Ag)-presenting functions. In mice, conventional DCs are divided into two subsets: CD11b-like and CD8α-like DCs. The division of conventional DCs into these two subsets is conserved across mammalian species, including human (Vu Manh et al., 2015a,b). All CD8α-like DCs specifically express the chemokine receptor XCR1. Therefore, CD8α-like DCs can be referred to as XCR1$^+$ DCs.

The function of DCs in priming naive T cells for promoting protective antiviral or antitumoral immunity is undisputable, as demonstrated by studies using mouse models to specifically deplete or conditionally inactivate genes in DCs (Bar-On and Jung, 2010a). In mice, XCR1$^+$ DCs encompass CD8α$^+$ DCs, which reside in lymphoid organs, and CD11b$^-$CD103$^+$ DCs, which reside in nonlymphoid tissues but migrate into draining lymph nodes to convey peripheral Ag to naive T cells. XCR1$^+$ DCs excel at priming effector CD8$^+$ T cells, including through uptake and processing of exogenous Ag for their presentation in association with major histocompatibility class (MHC) I molecules, a process called Ag cross-presentation (Vu Manh et al., 2015a). Upon primary response resolution, activated CD8$^+$ T cells contract and give rise to a pool of long-lasting memory CD8$^+$ T lymphocytes (mCTLs), that can swiftly and efficiently up-regulate effector functions upon antigen reexposure (Whitmire et al., 2008). Although this has been disputed (Belz et al., 2007; Mehlhop-Williams and Bevan, 2014), the antigen threshold necessary for the activation of memory or previously stimulated (Ag-experienced) T cells is thought to be lower than that for naive T cells. Indeed, in Ag-experienced T cells, including mCTLs, the signaling downstream of the TCR has been rewired for enhanced sensitivity to Ag binding (Farber, 2009; Kumar et al., 2011) and lower requirement on co-stimulation (Pihlgren et al., 1996; Curtsinger et al., 1998; London

*K. Crozat and M. Dalod contributed equally to this paper.

Correspondence to Karine Crozat: crozat@ciml.univ-mrs.fr; or Marc Dalod: dalod@ciml.univ-mrs.fr

Y.O. Alexandre's present address is Dept. of Microbiology and Immunology, The University of Melbourne, Peter Doherty Institute for Infection and Immunity, Parkville, VIC 3010, Australia.

Abbreviations used: Ag, antigen; CLN, cutaneous lymph nodes; DT, diphteria toxin; hDTR, human diphtheria toxin receptor; LCMV, lymphocytic choriomeningitis virus; *Lm*, *Listeria monocytogenes*; MCMV, mouse cytomegalovirus; mCTLs, memory CD8$^+$ T lymphocytes; MHC, major histocompatibility complex; RP, red pulp; tdTomato, tandem dimer Tomato; VSV, vesicular stomatitis virus; VV, Vaccinia virus; WP, white pulp.

The Rockefeller University Press $30.00
J. Exp. Med. 2016 Vol. 213 No. 1 75–92
www.jem.org/cgi/doi/10.1084/jem.20142350

et al., 2000; Rogers et al., 2000). Hence, contrary to naive T cells, Ag-experienced T cells can respond to Ag presentation by cells other than DCs, not only by other professional Ag-presenting cells, such as B cells or monocytes/macrophages, but also (and most importantly) directly by their target cells in nonlymphoid tissues, i.e., infected nonimmune cells or tumor cells (Croft et al., 1994; Dengler and Pober, 2000; Macleod et al., 2014). However, the cell types, signals, and molecular cascades driving optimal recall effector responses of mCTLs remain ill defined. In vivo, $CD11c^+$ cells help in activating mCTLs after secondary infections (Zammit et al., 2005). However, these cells include not only DCs but many other cell types (Probst et al., 2005; Bar-On and Jung, 2010b). In vitro, isolated splenic $XCR1^+$ DCs and $CD11b^+$ DCs induce mCTL proliferation with the same efficiency (Mehlhop-Williams and Bevan, 2014). When comparing the capacity of tumor-isolated myeloid cell types to activate naive or Ag-experienced T cells, $XCR1^+$ DCs are more proficient (Broz et al., 2014). Therefore, whether $XCR1^+$ DCs or other antigen-presenting cells are necessary for optimal reactivation of memory T cells in vivo remains unknown.

Several mutant mouse models have been developed to dissect the contribution of $XCR1^+$ DCs to immune responses in vivo. Some of these models were based on genetic inactivation of transcription factors critical for the ontogeny of $XCR1^+$ DCs such as ID2 (inhibitor of DNA binding), NFIL3 (nuclear factor, IL-3 regulated), IRF8 (IFN regulatory factor 8), and BATF3. Mice deficient for ID2, NFIL3, and IRF8 are affected in the ontogeny or functions of many cell types besides $XCR1^+$ DCs (Seillet and Belz, 2013). The penetrance of BATF3 mutation with regard to $XCR1^+$ DC development is incomplete on the *C57BL/6J* genetic background (Edelson et al., 2011b; Seillet et al., 2013; Mott et al., 2015). Other mouse models were designed to target $XCR1^+$ DCs based on the expression of the human diphtheria toxin (DT) receptor (hDTR) under the control of the *Langerin*, *Clec9a*, *Cd205*, or *Xcr1* genes. However, *Langerin*, *Clec9a*, and *Cd205* are not specifically expressed in $XCR1^+$ DCs (Jiang et al., 1995; Sancho et al., 2008; Schraml et al., 2013). Hence, administration of DT in *Clec9a-hDTR*, *Langerin-hDTR*, or *Cd205-hDTR* mice depletes other cell types, including other DC subsets (Kissenpfennig et al., 2005; Fukaya et al., 2012; Piva et al., 2012). The only mutant mouse model reported so far that specifically targets $XCR1^+$ DCs is the *Xcr1-hDTR-venus* mouse (Yamazaki et al., 2013). We present an alternative mutant mouse model, named *Karma*, which allows specific in vivo fluorescent tracking and ablation of $XCR1^+$ DCs.

Here, we used *Karma* memory mice to transiently eliminate $XCR1^+$ DCs, and investigate the involvement of these cells in the reactivation of mCTLs upon secondary infections with several pathogens. We found that $XCR1^+$ DCs are necessary for optimal expansion of mCTLs upon secondary infections with *Listeria monocytogenes* (*Lm*), Vaccinia virus (VV), or vesicular stomatitis virus (VSV), but not in the case of murine cytomegalovirus (MCMV). $XCR1^+$ DCs promote recall of mCTLs as early as a few hours after infection with *Lm*, independently of the role of these cells as bacterial vehicles. Our results show that reactivation of mCTLs in this context relies on their interactions with $XCR1^+$ DCs, a mechanism that depends on IFN-γ–dependent induction of IL-12 and CXCL9 in $XCR1^+$ DCs, and in part on CXCR3 engagement on mCTLs. In addition, NK cells are very rapidly activated upon secondary infection and serve as an early IFN-γ source, increasing the ability of $XCR1^+$ DCs to promote the reactivation of mCTLs.

RESULTS

Specific tracking and efficient conditional depletion of $XCR1^+$ DCs in *Karma* mice

Comparative gene expression profiling of mouse immune cells identified several genes as specifically expressed by $XCR1^+$ DCs, in particular the *a530099j19rik* gene (Fig. 1 A; Robbins et al., 2008; Crozat et al., 2011; Miller et al., 2012). We used this gene for knock-in of a construct encoding both the fluorescent tandem dimer Tomato (tdTomato) and the hDTR (Fig. 1 B) to generate a mouse model, named hereafter *Karma*, allowing specific tracking and conditional depletion of $XCR1^+$ DCs in vivo.

In *Karma* mice, all the tdTomato-positive splenocytes fell exclusively into the $XCR1^+$ subset of DCs as they expressed high level of CD11c and XCR1 (Fig. 2 A). More than 95% of splenic $XCR1^+$ DCs stained positive for tdTomato (Fig. S1 A and Fig. 2 B). In the dermis (Fig. S1 B) and lungs (unpublished data), tdTomato expression was the highest in the $XCR1^+$ subset of DCs (defined as $CD24^+CD103^+$ DCs; Fig. 2 C). In cutaneous lymph nodes (CLN; Fig. S1 C), tdTomato expression was the highest in both lymphoid tissue-resident and dermis-derived $XCR1^+$ DCs, and was low on migratory LCs (Fig. 2 D). Hence, the expression pattern of tdTomato in the *Karma* mouse model confirmed efficient targeting of all migratory and lymphoid-resident $XCR1^+$ DCs.

We next evaluated the specificity and efficiency of $XCR1^+$ DC conditional depletion in *Karma* mice. The administration of a single dose of DT was sufficient to eliminate >95% of splenic $XCR1^+$ DCs within 6 h without affecting other immune cells (Fig. 2, E and F). In the spleen, the compartment of $XCR1^+$ DCs was emptied for at least 2 d and fully recovered by day 4 after DT treatment (Fig. 2 F). DT administration also induced an efficient elimination of $XCR1^+$ DCs found in the dermis and in the CLNs (unpublished data). The efficiency of $XCR1^+$ DC depletion in DT-treated *Karma* mice was functionally confirmed by two types of assays. First, $CD11c^+$ cells purified from the spleens of OVA-injected and DT-treated *Karma* mice failed to cross-present OVA to naive $CD8^+$ T cells in vitro (Fig. 2 G). Second, DT-treated *Karma* mice failed to produce bioactive IL-12 upon administration of *Toxoplasma gondii*–soluble tachyzoïte antigen (STAg; Fig. 2 H), which specifically triggers IL-12 production in $XCR1^+$ DCs through TLR11 (Yarovinsky et al., 2005). Hence, the *Karma* mouse model is a robust in vivo system that allows a selective depletion of $XCR1^+$ DCs.

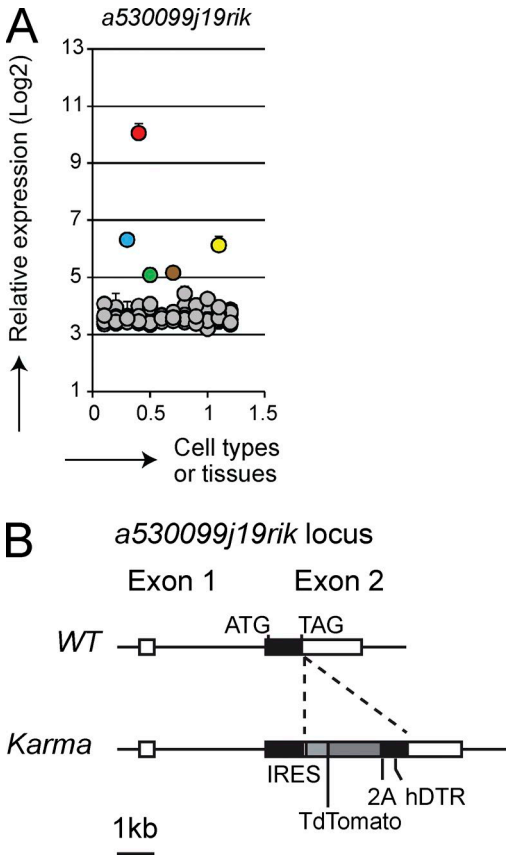

Figure 1. **Expression analysis of the *a530099j19rik* gene and generation of *Karma* mice.** (A) Microarray analysis of the expression of the *a530099j19rik* gene in 96 different cell types or tissues in mouse. pDCs (green), CD11b$^+$ (blue), and XCR1$^+$ (red) DCs, spleen (brown), and lymph nodes (yellow) are highlighted among all other cell types and tissues (gray). (B) Schematic representation of the *Karma* mouse genetic construction. An IRES-tdTomato-2A-DTR cassette was inserted downstream of the stop codon in the 3′ untranslated region of exon 2 of the *a530099j19rik* gene.

XCR1$^+$ DCs promote the expansion of mCTLs upon secondary infections with several intracellular pathogens

We used *Karma* mice to investigate whether XCR1$^+$ DCs are required to promote the recall of mCTLs. Upon immunization with *Lm-OVA*, *Karma* mice generated a pool of long-lived mCTLs quantitatively and qualitatively comparable to those of WT mice (unpublished data). Memory DT-treated *Karma* mice were then secondary challenged with different OVA-expressing recombinant microbes: the bacteria model *Lm* (*Lm-OVA*), mouse cytomegalovirus (MCMV-OVA), VV (VV-OVA), or VSV (VSV-OVA). Upon secondary infection with *Lm*-OVA, VV-OVA, and VSV-OVA, a sustained depletion of splenic XCR1$^+$ DCs strongly decreased the numbers of Ag-specific mCTLs found in the spleen of *Karma* mice 5 d after rechallenge (Fig. 3, A and B; and Fig. S2 A). XCR1$^+$ DCs also promoted the expansion of OVA-specific mCTLs when VSV-OVA or VV-OVA were used as immunizing agents (Fig. 3 A). Hence, the XCR1$^+$ DC-mediated recall response of mCTLs is not specific to primary or secondary infections by *Lm*, but also occurs with several other infectious agents. Because the effect of XCR1$^+$ DC depletion was more drastic for *Lm-OVA* than for VSV-OVA or VV-OVA secondary infections, we focused on *Lm-OVA* infection to define the critical time frame during which XCR1$^+$ DCs mediate the reactivation of mCTLs. We therefore administered DT to memory *Karma* mice at different times around secondary challenge. An early and transient depletion of XCR1$^+$ DCs, starting before secondary infection and lasting for ∼1.5 d after, significantly prevented expansion and effector functions of mCTLs (Fig. 3 C). In contrast, a late and sustained depletion of XCR1$^+$ DCs starting 1 d after infection had no effect on the recall of mCTL responses (Fig. 3 D). Because the intensity of the immune response to OVA-recombinant microbes may not reflect the immune response to Ag naturally existing in the pathogen, we analyzed the activation of mCTLs specific of an endogenous epitope of *Lm* (Listeriolysin peptide $LLO_{296-304}$) in a context of an autologous secondary infection (Fig. 3 E). We also examined responses against the nucleoprotein NP_{396} epitope endogenous to the lymphocytic choriomeningitis virus (LCMV) immunizing agent upon a heterologous secondary infection with VV-NP (unpublished data). In both cases, XCR1$^+$ DCs promoted the recall of mCTLs specific to endogenous Ag (Fig. 3 E and not depicted). Hence, the role of XCR1$^+$ DCs for promoting the recall of antigen-specific mCTLs is not limited to the OVA model epitope but applies to different antigens, including endogenous epitopes of the immunizing or challenging infectious agent. We then studied how XCR1$^+$ DCs are required to promote mCTL recall within the first day after rechallenge using OVA as a model of Ag and OVA-expressing *Lm* for primary and secondary infections.

XCR1$^+$ DCs promote the early activation of mCTLs upon secondary infection with *Listeria*

As early as 8 h after *Lm* rechallenge, mCTLs produce IFN-γ, in an Ag-independent fashion (Berg et al., 2003; Bajénoff et al., 2010; Soudja et al., 2012). We therefore analyzed whether depletion of XCR1$^+$ DCs influenced this first, early phase of mCTL reactivation. To follow the behavior of Ag-specific CD8$^+$ T cells in our experimental model, we injected low numbers (500–1,000) of naive GFP-expressing OT-I cells before each primary infection, to mimic the preimmune frequency of individual antigen-specific CD8$^+$ T precursors present at steady state in a mouse (Obar et al., 2008). Upon secondary infections, depletion of splenic XCR1$^+$ DCs abrogated the early induction of IFN-γ in both OVA-specific OT-I mCTLs (Fig. 4 A and Fig. S2 B) and endogenous polyclonal Ag-experienced CD44^{hi} CD8$^+$ T cells (CD44^{hi} mCTLs; Fig. 4 B and Fig. S2 B) without significantly affecting their expression of Granzyme B.

Upon primary infection with *Lm*, XCR1$^+$ DCs convey bacteria from the red pulp (RP) to the white pulp (WP) in the spleen, which conditions the delivery of *Lm*-derived Ag

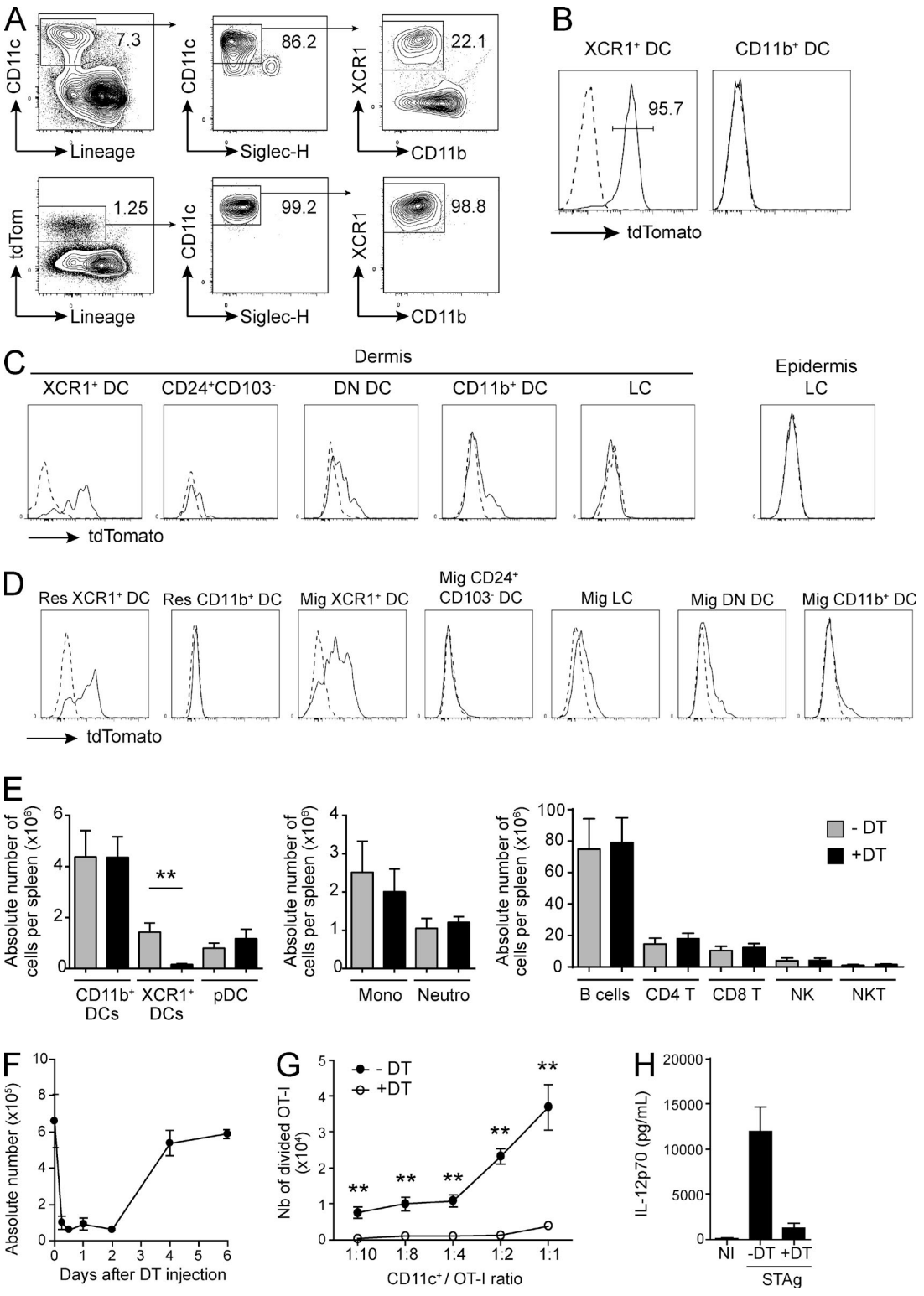

Figure 2. **In *Karma* mice, all XCR1$^+$ DCs express the tdTomato, and are specifically and efficiently depleted upon DT administration.** (A) Analysis of the tdTomato expression among total splenocytes. After dead cell exclusion, tdTomato-positive cells were analyzed for lineage (CD3ε/CD19/NK1.1), CD11c, SiglecH, XCR1, and CD11b expression. The percentage of cells among the gate is shown. (top) Gating strategy using control splenocytes; (bottom) staining of *Karma* splenocytes. (B–D) Analysis of tdTomato expression by DCs in spleen (B), epidermis and dermis (C), and CLNs (D) of *Karma* mice. See Fig. S1 (A–C) for details about the gating strategy used. WT cells (dotted histogram) were included in overlays to set the tdTomato background signal for com-

to naive T cells and subsequent induction of protective $CD8^+$ T cell responses (Neuenhahn et al., 2006; Aoshi et al., 2008; Campisi et al., 2011; Edelson et al., 2011a). Upon secondary infection, *Lm* may also use $XCR1^+$ DCs to disseminate into the spleen, which may strongly decrease antigen load in mice depleted of $XCR1^+$ DCs and thus explain their strongly diminished mCTL responses. Bacterial loads were 6.6 times lower in $XCR1^+$ DC-depleted animals than in controls 6 h after infection (Fig. 4 C), confirming that $XCR1^+$ DCs promote bacterial spreading in the spleen. Yet thousands of colony-forming units were readily detected in the spleen of $XCR1^+$ DC-depleted mice, indicating that the amount of replicative bacteria was unlikely to be a limiting factor for the reactivation of mCTLs in the absence of $XCR1^+$ DCs. To test this hypothesis, we used CFSE-stained UV-irradiated *Lm-OVA*, which lack replicative capacity because of UV-induced DNA damages, but which retain intact structural components preserving their immunogenicity, unlike heat-killed bacteria (Muraille et al., 2005). Although similar bacterial loads were observed in both memory DT-treated and untreated *Karma* mice injected with UV-irradiated *Lm-OVA* (Fig. 4 D), the induction of IFN-γ in polyclonal $CD44^{hi}$ mCTLs was significantly lower in DT-treated *Karma* mice (Fig. 4 E). Therefore, independent of shuttling live bacteria, $XCR1^+$ DCs must exert specific immune functions, which promote mCTL responses within the first hours after secondary challenges. This prompted us to investigate the mechanisms by which $XCR1^+$ DCs promoted the reactivation of mCTLs early after secondary infection.

$XCR1^+$ DCs promote mCTL clustering in the RP early after *Lm* infection

We first investigated whether the depletion of $XCR1^+$ DCs impacted the migration of mCTLs, which occurs very early after secondary *Lm* infection (Bajénoff et al., 2010). Under steady-state conditions, mCTLs mostly resided in the RP of the spleen (Fig. 5 A, NI). Within the first hours after secondary infection, they transiently formed clusters around B cell follicles (Fig. 5 A, 6 h −DT) before migrating into the T cell zone (Fig. 5 A, 24 h −DT). The depletion of $XCR1^+$ DCs before secondary infection significantly decreased but did not completely abrogate the early clustering of mCTLs (Fig. 5, A [6 h +DT] and B) and their later migration into the T cell zone (Fig. 5, A [24 h +DT] and C).

We then examined the microanatomical localization of $XCR1^+$ DCs in the spleen upon secondary infection. At steady-state in *Karma* mice, $XCR1^+$ DCs were located in the RP and in the T cell zone (Fig. 6 A). 6 h after rechallenge, $XCR1^+$ DCs formed clear clusters together with OT-I mCTLs around the marginal zone (Fig. 6 A). IFN-γ–producing cells, which encompassed a significant proportion of memory OT-I cells, were strictly confined within these clusters (Fig. 6 B). 24 h after infection, the proportion of $tdTomato^+$ cells was more prominent in the T cell zone as compared with the RP, suggesting that a proportion of $XCR1^+$ DCs that initially resided in the RP, most probably those clustering with mCTLs at 6 h, entered the WP at 24 h (Fig. 6 A). Altogether, these results showed that the responses of $XCR1^+$ DCs during *Lm-OVA* secondary infection were tightly regulated in time and space and promoted mCTL clustering and IFN-γ production in the RP, at the edges of the marginal zone.

$XCR1^+$ DCs secrete IL-12 and CXCL9, which respectively promote the activation and mobilization of mCTLs

To gain insights into the mechanisms through which $XCR1^+$ DCs promoted the recall of mCTLs early after secondary infection, we compared the expression of genes encoding candidate inflammatory cytokines and chemokines in the spleen of DT-treated versus untreated *Karma* mice after *Lm* rechallenge. The expressions of *Il12b* and *Cxcl9* genes were significantly reduced in DT-treated mice as early as 3 h after infection (unpublished data). Upon secondary infection of memory mice, $XCR1^+$ DCs were a major source of IL-12p40/70 as compared with $CD11b^+$ DCs, neutrophils, and monocytes (Fig. 7 A and Fig. S3, A and B). The blockade of IL-12 before secondary inoculation with *Lm-OVA* drastically impaired IFN-γ induction in OT-I (Fig. 7 B) and polyclonal $CD44^{hi}$ (Fig. 7 C) mCTLs, suggesting that IL-12 provides the very first signal that initiates their reactivation. $XCR1^+$ DCs were also the major producers of CXCL9 6 h after secondary challenge (Fig. 7 D and Fig. S3 C). CXCL9 staining colocalized strongly with clusters of $XCR1^+$ DCs in the spleen of memory mice (Fig. 7 E). Therefore, early after secondary infection, $XCR1^+$ DCs are the major source of IL-12 and CXCL9.

In *C57BL/6J* mice, CXCL9 and CXCL10 specifically bind the chemokine receptor CXCR3, which is mostly expressed on Ag-experienced effector and memory T cells (Qin et al., 1998; Rabin et al., 1999). Upon *Lm* secondary infection, CXCR3 expression was down-regulated on $CD44^{hi}$ T lymphocytes, and more profoundly on the $CD8^+$ subset

parison with *Karma* cells (black histogram). For the spleen, one experiment representative of at least four with three mice per group is shown. For the skin and CLNs, one representative experiment out of three with three mice per group is shown. (E and F) Specific depletion and recovery of $XCR1^+$ DCs in *Karma* mice upon DT administration. Splenocytes of DT-injected mice were analyzed by flow cytometry 24 h (E) or several days after treatment (F). The absolute numbers of the analyzed cell population are represented. In these experiments, $XCR1^+$ DCs were gated using CD8α staining in place of XCR1. Data are shown for one experiment representative of two independent ones, with three mice per group. (G) Antigen cross-presentation is abolished in $XCR1^+$ DC-depleted mice. Data are shown for one experiment representative of two with three mice per group. Data are represented as mean ± SEM. **, $P < 0.01$. (H) IL-12p70 induction is reduced in $XCR1^+$ DC-depleted mice upon STAg administration. The experiment was performed with two noninjected (NI) control mice, and with three STAg-injected mice per condition. Data are represented as mean ± SEM.

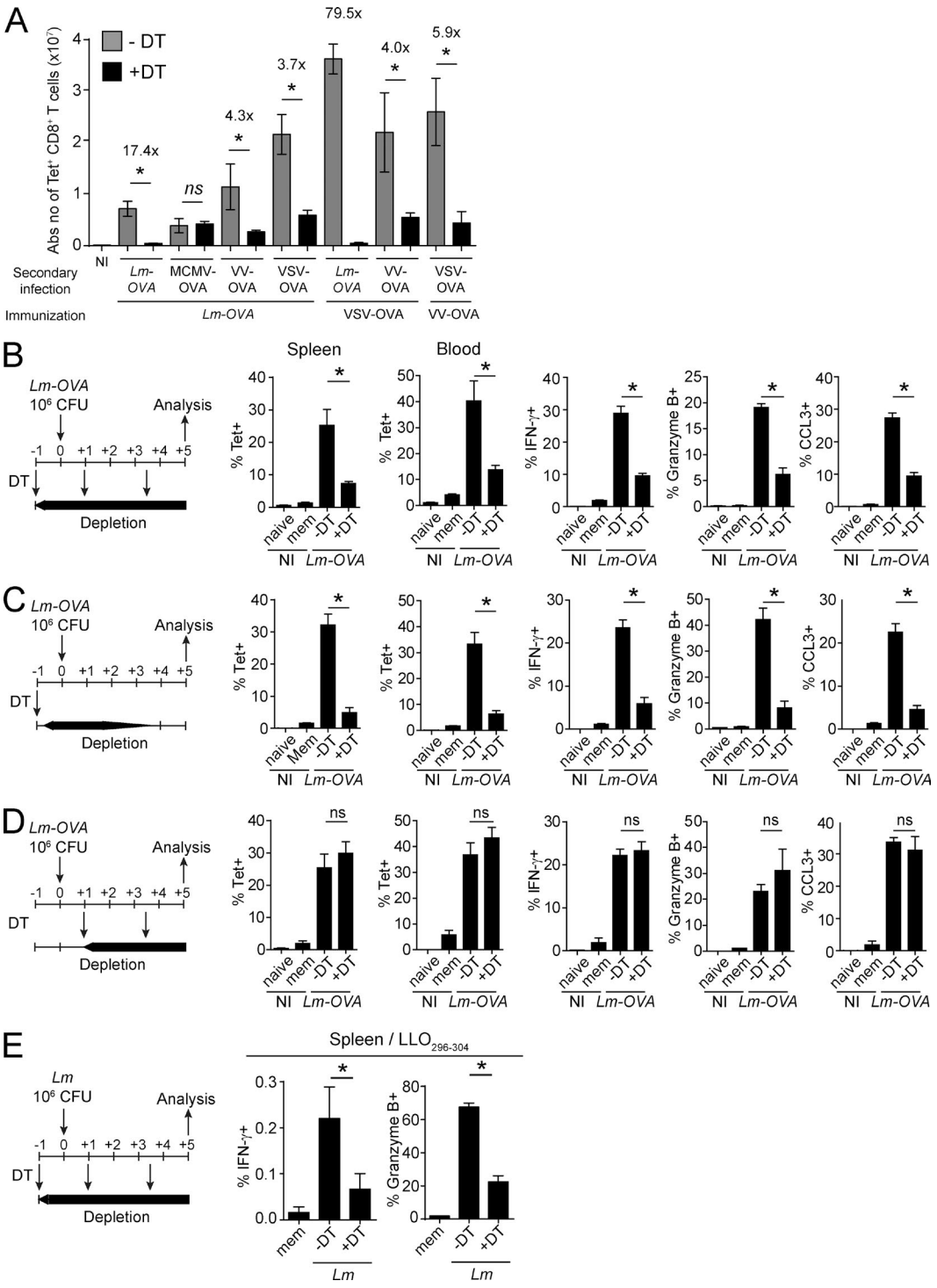

Figure 3. **Splenic XCR1⁺ DCs promote mCTL responses upon secondary infection with various intracellular pathogens.** Memory mice were used 30 d after primary infections. (A) The DT was injected 1 d before, and 1 and 3.5 d after secondary infections with *Lm-OVA*, MCMV-OVA, VV-OVA, or VSV-OVA. Tetramer-positive cells were measured by flow cytometry 5 d after infections. See Fig. S2 for the detailed gating strategy. Graph shows pooled data (mean ± SEM) from two independent experiments each with two to three mice per group. *, $P < 0.05$; ns, not significant. NI, noninfected. (B–D) Different protocols of DT treatment were applied as illustrated. DT was injected 1 d before, and 1 and 3.5 d after (B), or 1 d before (C), or 1 and 3.5 d after (D) secondary infection with 10^6 CFU of *Lm-OVA*. Splenocytes and blood leukocytes were analyzed by flow cytometry 5 d after infection. IFN-γ, GzmB, and CCL3 induction was measured after in vitro restimulation with SIINFEKL. Data (mean ± SEM) are shown for one experiment representative of two with three to four mice per group (*, $P < 0.05$; ns, not significant). NI, noninfected. (E) Analysis of IFN-γ and GzmB induction in CD8⁺ T cells from the spleen of DT-treated memory *Karma*

than on the $CD4^+$ one (unpublished data). $CD44^{hi}$ $CD8^+$ T cells also migrated more efficiently than $CD44^{hi}$ $CD4^+$ T cells in response to CXCL9 in vitro (unpublished data). We therefore hypothesized that the clusters of CXCL9-producing $XCR1^+$ DCs observed in the spleen early after secondary infection recruited mCTLs through engagement of their CXCR3 receptors. In vivo blockade of CXCR3 before secondary inoculation with *Lm-OVA* significantly decreased the early production of IFN-γ by mCTLs (Fig. 7, F and G) and their clustering (Fig. 7 H).

Collectively, these results indicated that, within a few hours after secondary infection, $XCR1^+$ DCs secreted IL-12, which triggered IFN-γ production by mCTLs, and CXCL9, which participated in the attraction of mCTLs toward $XCR1^+$ DCs, and therefore in their activation.

Early IFN-γ production and NK cells promote the induction of CXCL9 and IL-12 in $XCR1^+$ DCs

One of the most potent inducers of CXCL9 expression is IFN-γ. In vivo neutralization of IFN-γ before *Lm-OVA* secondary infection reduced IL-12 and abrogated CXCL9 production by $XCR1^+$ DCs (Fig. 8 A), resulting in a decrease in the clustering of mCTLs (Fig. 8 B). Therefore, IFN-γ constitutes one of the first signals initiating the activation of mCTLs upon *Lm-OVA* secondary infection by (a) acting in a positive-feedback loop on $XCR1^+$ DCs to amplify IL-12 induction, and (b) inducing CXCL9 expression by $XCR1^+$ DCs, and the redistribution of mCTLs at the edges of marginal zones of the spleen.

Early after secondary infection, NK cells accounted for 40% of IFN-γ–expressing splenocytes (Fig. 8 C). At that time, IFN-γ–producing NK cells localized into cell clusters with $XCR1^+$ DCs and mCTLs around B cell follicles (Fig. 8, D and E, −DT). NK cell redistribution upon secondary infection depended on $XCR1^+$ DCs, as DT treatment of *Karma* mice affected their activation and clustering (Fig. 8, D and E, +DT). We therefore investigated the impact of NK cell depletion on the responses of $XCR1^+$ DCs and of mCTLs. NK cell-depleted memory mice harbored an almost complete loss of IL-12 induction in $XCR1^+$ DCs and a significant decrease in the expression of CXCL9 (Fig. 8 F). The induction of IFN-γ in mCTLs was also significantly decreased in these mice (Fig. 8, G and H). However, although slightly reduced, the number of clusters of mCTLs was not significantly altered in mice depleted of NK cells (Fig. 8 I). Thus, NK cells contact $XCR1^+$ DCs very rapidly during secondary infection and deliver signals that amplify the ability of $XCR1^+$ DCs to reactivate mCTLs through IL-12.

Impact of the depletion of $XCR1^+$ DCs on early mCTL responses during secondary challenge with VV-OVA

During secondary challenge with VV-OVA, the depletion of $XCR1^+$ DCs significantly decreased the early clustering of mCTLs around the marginal zone (Fig. 9 A) and NK cell IFN-γ (Fig. 9 B), similarly to, but less strongly than, what was observed upon autologous secondary challenges with *Lm-OVA*. Consistently with these observations, $XCR1^+$ DCs were a major source of IL-12 and CXCL9 a few hours after secondary infection (Fig. 9 C). These data suggest that the recall of mCTL responses to secondary infections with *Lm* and VV are promoted by $XCR1^+$ DCs through overlapping molecular and cellular mechanisms.

DISCUSSION

In this study, we described a new mouse model named *Karma*, which allows specific fluorescent tracking and efficient depletion of all $XCR1^+$ DCs. The *Karma* mouse was engineered using the *a530099j19Rik* gene to drive the expression of the tdTomato-hDTR cassette. This gene codes for a predicted G protein–coupled receptor of unknown function. Its expression is highly specific to $XCR1^+$ DCs throughout the body. Hence, the *Karma* mouse model is a good alternative to the recently described *Xcr1-hDTR-venus* mouse model (Yamazaki et al., 2013). We took advantage of the ability to specifically and conditionally deplete $XCR1^+$ DCs in the *Karma* mouse model to investigate the implication of these cells in mCTL responses to secondary infections by intracellular pathogens.

We established for the first time that $XCR1^+$ DCs are instrumental for the expansion of mCTLs upon VV-OVA, VSV-OVA, and *Lm-OVA* secondary challenges. The use of the CD11c-DTR mouse model has previously shown that mCTL recall responses to VSV, influenza, or *Lm* secondary infections were dependent on $CD11c^+$ cells (Zammit et al., 2005). Here, we have identified $XCR1^+$ DCs as the major cell subset involved in the reactivation of mCTLs upon VSV, VV, and *Lm* secondary infections. The amplitude of the defect previously observed in $CD11c^+$ cell-depleted animals was more drastic than what we report here in $XCR1^+$ DC-depleted individuals. This might be a result of differences in experimental conditions, specifically, the fact that we examined responses to endogenously induced mCTLs, whereas the study by Zammit et al. (2005) used adoptive transfer of mCTLs in naive animals before their challenge with autologous or heterologous pathogens. Alternatively, or in addition, numerous other $CD11c^+$ cell subsets than $XCR1^+$ DCs are known to be depleted in the CD11c-DTR model and some of these may also contribute to the secondary activation of mCTLs, including through production of IL-12, IL-18, IL-15, CXCL9, or CXCL10 (Sung et

mice 5 d after secondary challenge, after in vitro restimulation with $LLO_{296-304}$ peptide. *Lm-WT* was used for the primary (3×10^3 CFU) and secondary (10^6 CFU) infections. The protocol of DT administration applied was the same as in B. See Fig. S2 for the detailed gating strategy. Data (mean ± SEM) are shown for one experiment representative of two with three to four mice per group. *, $P < 0.05$; ns, not significant. NI, noninfected.

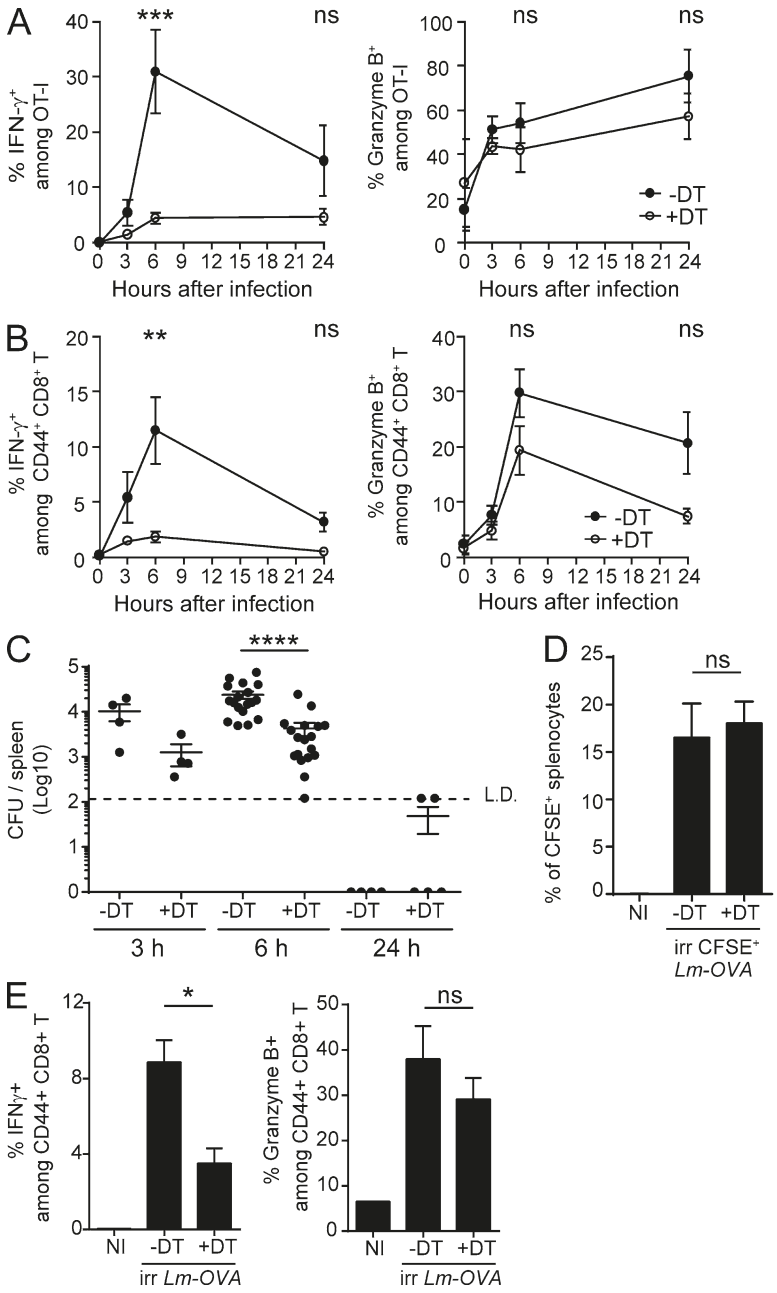

Figure 4. **XCR1⁺ DCs promote the early production of IFN-γ by mCTLs.** *Karma* mice received 500–1000 naive GFP⁺ OT-I cells 1 d before primary infection with *Lm-OVA*. 30 d later, mice were treated with DT (open circle) or left untreated (black circle), and secondary infected 1 d later with 10^6 CFU of *Lm-OVA*. Splenocytes were harvested, incubated with brefeldin A before intracellular staining of IFN-γ and GzmB. Fig. S2B contains details of the gating strategy. (A) Analysis of the activation of OT-I GFP⁺ mCTLs. ***, P < 0.001. (B) Analysis of IFN-γ and Granzyme B induction in all endogenous polyclonal mCTLs as identified by their $CD44^{hi}$ phenotype. Graph shows pooled data (mean ± SEM) from three independent experiments each with three mice per group. **, P < 0.01. (C) Bacterial load in DT-treated *Karma* mice after secondary infection with *Lm*. Enumeration of *Lm* in spleens of DT-treated and untreated memory *Karma* mice 3, 6, and 24 h after secondary infection; L.D., limit of detection. Data are represented as mean ± SEM. ****, P < 0.0001. Data at 6 h are pooled from five independent experiments each with at least three mice per group. Data at 3 and 24 h are pooled from two independent experiments each with two to three mice per group. (D and E) Memory DT-treated *Karma* mice were infected with 10^8 CFU of UV-C–treated CFSE-stained *Lm-OVA*. Analysis of CFSE⁺ splenocytes (D) and of IFN-γ and Granzyme B induction in all polyclonal $CD44^{hi}$ mCTLs in spleens (E) of mice 6 h after secondary infection with UV-C–irradiated bacteria. Data (mean ± SEM) are shown for one experiment representative of two with three to four mice per group. *, P < 0.05; ns, not significant. NI, noninfected.

al., 2012; Kastenmüller et al., 2013). During *Lm-OVA* secondary infection, XCR1⁺ DCs were required for the early production of IFN-γ by mCTLs, which was previously reported to be independent of cognate antigen–specific interactions. We further deciphered the mechanisms by which XCR1⁺ DCs promote mCTL recall during secondary *Lm-OVA* infection. As during primary infection, the first cells in the spleen that host live bacteria upon *Lm* secondary challenge are most likely XCR1⁺ DCs. In our study, we used a high dose of *Lm-OVA* (10^6 CFU) for secondary challenge such that live bacteria could be readily detected in the spleen of XCR1⁺ DC-depleted animals. This implies that other cell types hosted the pathogen, such as monocytes that can be infected by *Lm* (Muraille et al., 2007; Edelson et al., 2011a). We also made use of UV-irradiated bacteria, which failed to actively replicate, to obtain the same level of infection in both XCR1⁺ DC-depleted and control animals. The loss of XCR1⁺ DCs led to a significant reduction of mCTL recall under conditions of similar antigenic loads between treated and control animals. Altogether, our results support a mechanism whereby the activation of mCTLs during *Lm* secondary infection is promoted by their involvement in a ménage à trois with XCR1⁺ DCs and NK cells acting as an amplification loop for the activation of all three partners (Fig. S4).

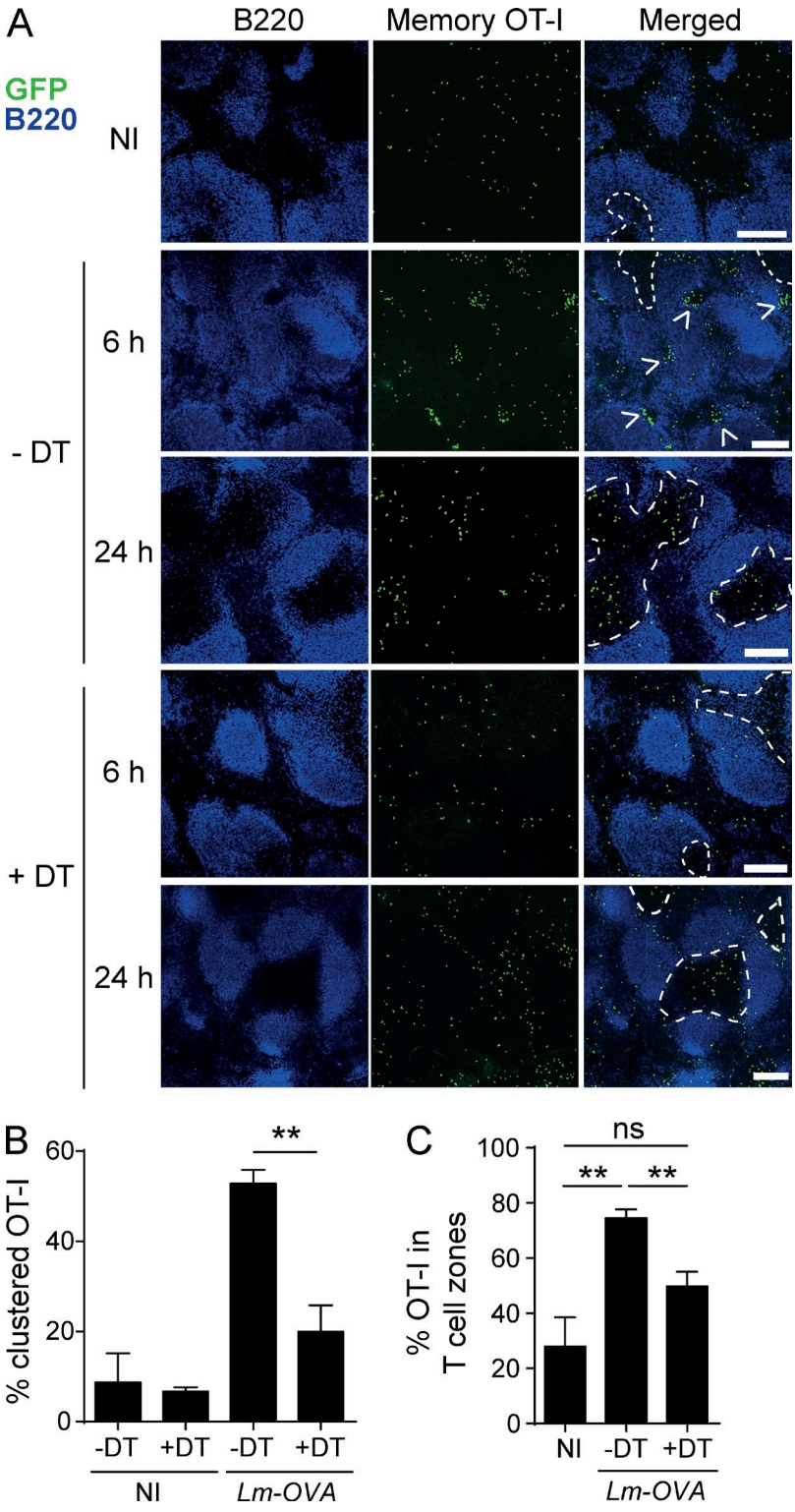

Figure 5. **XCR1$^+$ DCs are required for the clustering of mCTLs around the marginal zone, and promote their subsequent migration into the T cell zone.** Memory *Karma* mice were generated as described in Fig. 3. (A) Spleen sections from untreated or DT-treated memory mice were stained with anti-B220 (dark blue) and anti-GFP (green) to define B cell follicles and OT-I mCTLs, respectively, and analyzed by confocal microscopy. Bars, 200 µm. Dotted lines delineate T cell zones. One representative experiment of three, each with three mice per group, is shown. (B) Statistical analysis of the frequency of OT-I mCTLs found clustered around the follicles at 6 h. Graph shows pooled data (mean ± SEM) from three independent experiments each with three mice per group. **, $P < 0.01$. (C) Statistical analysis of the frequency of OT-I mCTLs present in the T cell zones at 24 h. Graph shows pooled data (mean ± SEM) from two independent experiments each with three mice per group. **, $P < 0.01$; ns, nonsignificant.

Besides being involved in the early activation of mCTLs upon *Lm-OVA* secondary infection through IL-12 and CXCL9 production, XCR1$^+$ DCs also have a critical role in the expansion of mCTLs, which occurs later during the recall response. We demonstrated that XCR1$^+$ DCs were critical within the first days after infection to promote this phenomenon. How XCR1$^+$ DC early functions influence the late expansion of mCTLs remains unknown. Several scenarios

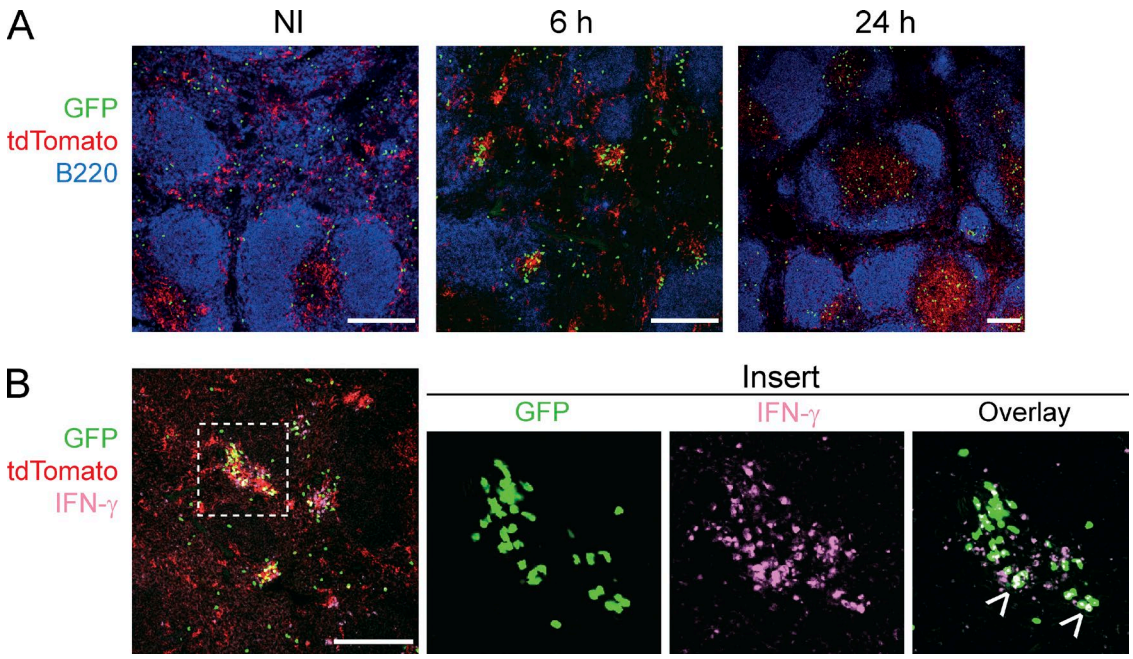

Figure 6. **RP-associated XCR1⁺ DCs form clusters around the marginal zone and activate mCTLs.** Memory *Karma* mice were generated as described in Fig. 3. Anti-GFP (green) and anti-dsRed (red) antibodies were used to detect memory OT-I cells and tdTomato⁺ XCR1⁺ DCs, respectively, on spleen sections imaged by confocal microscopy. (A) Spleen sections were stained with anti-B220 (dark blue) to define B cell follicles. (B) IFN-γ staining (pink) of spleen sections 6 h after secondary *Lm-OVA* infection. Overlay of IFN-γ staining with GFP gave a white color (arrows in insert). One representative experiment out of three with three mice per group is shown. Bars, 200 µm.

are possible. First, XCR1⁺ DCs may promote mCTL expansion through the secretion of soluble factors. We found that IL-12 and CXCL9 did not seem to be required (unpublished data). However, other molecules, such as the IL-15–IL-15Rα complex, which has strong proliferative properties on memory cells (Richer et al., 2015), may be important. Second, XCR1⁺ DCs may promote mCTL expansion through MHC class I–restricted Ag presentation. Third, XCR1⁺ DCs may promote mCTL expansion by recruiting the help of a third cell partner. Although, in our experimental setting, NK cells clustered with XCR1⁺ DCs and mCTLs, the expansion of mCTLs still occurred when NK cells were depleted (unpublished data). However, we cannot exclude that other cells may also form clusters with XCR1⁺ DCs and mCTLs and contribute to promoting the expansion of the latter. Two recent studies have shown that tripartite interactions between XCR1⁺ DCs, CD4⁺ T cells, and primed CD8⁺ T cells are critical during primary viral infections to promote the expansion of the latter and their differentiation in protective mCTLs (Eickhoff et al., 2015; Hor et al., 2015). XCR1⁺ DCs physically interact with both CD4⁺ and CD8⁺ T cells, either sequentially when the infectious agent does not reach the lymphoid organs and remains confined in the peripheral tissues (Hor et al., 2015), or concomitantly, forming tripartite clusters when the pathogen directly infects cells within the lymphoid tissues (Eickhoff et al., 2015). In our experimental model, upon secondary infection with *Lm-OVA*, CD4⁺ T cell activation was attenuated when XCR1⁺ DCs were absent (unpublished data). Therefore, as for primary infections, CD4⁺ T cells could form clusters with XCR1⁺ DCs and mCTLs to deliver a help signal necessary to promote the reactivation and expansion of mCTLs.

Recently, in an experimental system similar to ours, Soudja et al. (2012) reported that Ly6C⁺CCR2⁺ monocytes were also required for this function in *Lm-OVA* secondary-infected animals. Combining these two studies thus raises the question of the respective contributions of XCR1⁺ DCs and monocytes in the promotion of mCTL responses upon secondary infection with *Lm*. To deplete monocytes, they used *Ccr2-hDTR* mice (Soudja et al., 2012). Although particularly high on classical monocytes, CCR2 is also expressed on cDCs, plasmacytoid DCs, nonclassical monocytes, activated CD4⁺ and CD8⁺ T cells, and NK cells (Mack et al., 2001; Heng and Painter, 2008; Elpek et al., 2011; van Helden et al., 2012). Indeed, DT treatment of *Ccr2-hDTR* mice eliminates not only classical monocytes but also a proportion of plasmacytoid DCs, XCR1⁺ DCs, and CD11b⁺ DCs (Shi et al., 2011; Dutertre et al., 2014). Hence, the alteration of mCTL responses observed in CCR2⁺ cell-depleted animals could result from the combined depletion not only of classical monocytes but also of other immune cells, including a fraction of XCR1⁺ DCs. Clusters of CCR2⁺ cells and mCTLs are formed in the RP of the spleen as soon as 8 h after infection (Soudja et al., 2012). Interestingly, upon *Lm-OVA* secondary

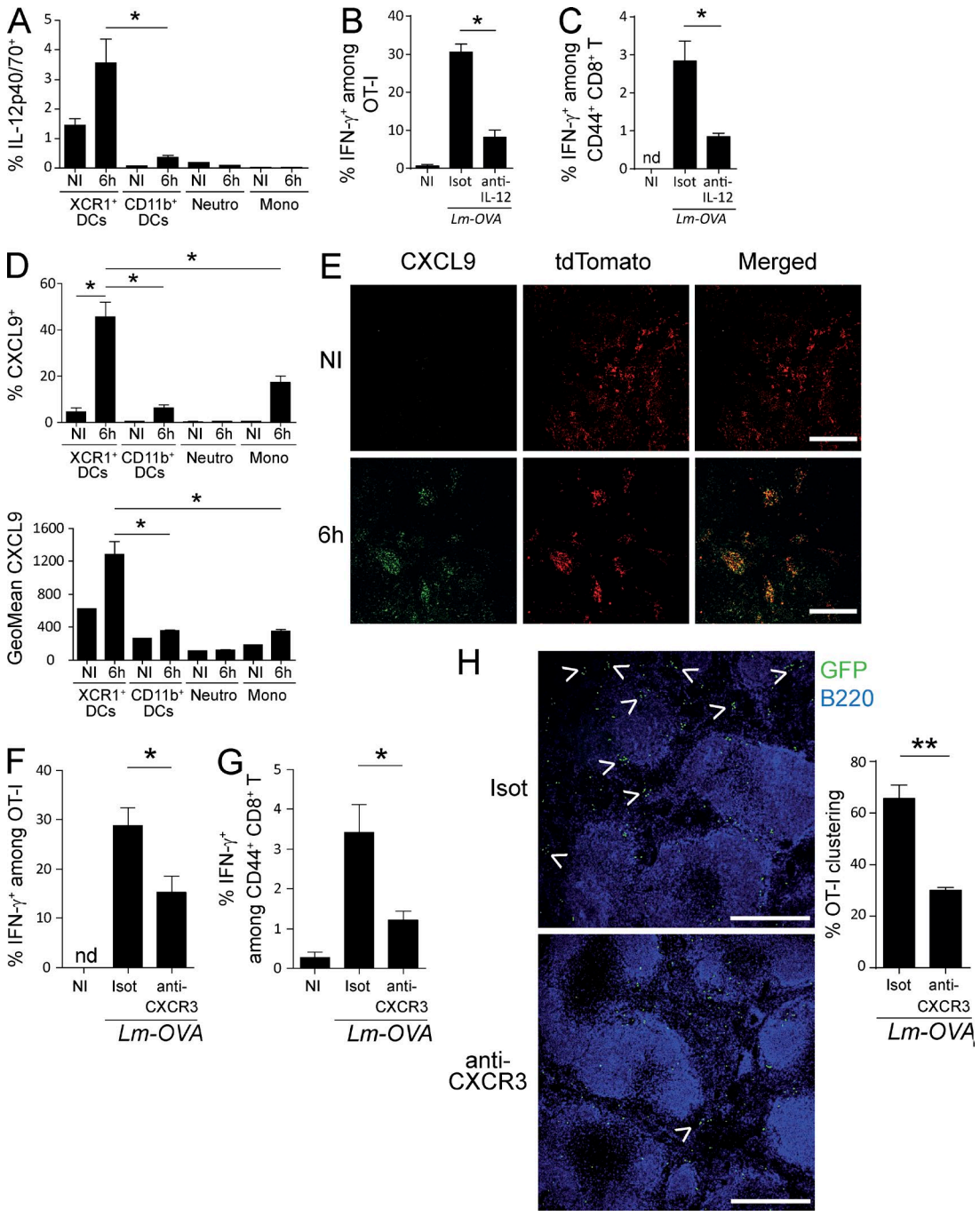

Figure 7. **Role of IL-12 and CXCL9 production by XCR1⁺ DCs in the early recruitment and activation of mCTLs after secondary infection.** The induction of IL-12p40/70 (A) and CXCL9 (D) was analyzed by flow cytometry 6 h after *Lm-OVA* rechallenge in several splenocyte populations (see Fig. S3 for the detailed gating of cells). IL-12p40/70 and CXCL9 were not detected in any other populations than cDC subsets, neutrophils, and monocytes. Intracellular staining was performed directly ex vivo without prior incubation with brefeldin A. Data (mean ± SEM) are shown from one experiment representative of three independent ones, each with at least three mice per group. *, $P < 0.05$. (B and C) IL-12 neutralization abrogates IFN-γ induction in mCTLs upon secondary infection. Memory mice were treated with IL-12–blocking antibody (anti–IL-12) or isotype control (Isot) 18h before secondary infection. Spleens were harvested at 6 h after secondary *Lm-OVA* infection. Frequency of OT-I mCTLs (B) and of polyclonal $CD44^{hi}$ mCTLs (C) that produce IFN-γ 6 h post-secondary infection was measured as in Fig. 4. Data (mean ± SEM) are from one experiment with at least four mice per group. *, $P < 0.05$. (E) Spleen sections of memory *Karma* mice either noninfected (NI) or infected for 6 h with *Lm-OVA* (6 h), were stained with anti-CXCL9 (green) and anti-dsRed (red). Merged image shows overlay of anti-CXCL9 with anti-dsRed. Bar, 200 µm. One representative experiment of two, each with two mice per group, is shown. (F–H) Memory mice were treated with CXCR3-blocking antibody (anti-CXCR3) or isotype control (Isot) 18 h before secondary infection. Spleens were harvested at 6 h after

infection, XCR1$^+$ DCs promote the induction of the CCR2 ligands CCL2 and CCL7 (unpublished data). Therefore, XCR1$^+$ DCs may participate in the attraction of monocytes in their closed vicinity, favoring cell–cell contacts and promoting an optimal inflammatory milieu to mCTLs. Functionally, XCR1$^+$ DCs and classical monocytes likely mediate distinct and complementary functions for the reactivation of mCTLs. XCR1$^+$ DCs are the main producers of CXCL9 and IL-12, which promotes the local recruitment of mCTLs and their early IFN-γ production but does not affect their expression of the cytolytic molecule Granzyme B. Classical monocytes are the main producers of IL-15/IL15Rα, which promotes the acquisition of cytolytic functions by mCTLs (Soudja et al., 2012). The later expansion of mCTLs upon secondary infection might also depend on complementary functions of classical monocytes and XCR1$^+$ DCs, for example IL-15 transpresentation by the former and cross-presentation of *Lm* antigens by the later.

We showed that upon secondary challenge NK cells account for a large amount of early IFN-γ, which promoted IL-12 and CXCL9 production by XCR1$^+$ DCs and their downstream capacity to activate mCTLs. To our knowledge, a role of NK cells in the promotion of the recall of mCTLs has never been reported. Upon primary inoculation with *Lm*, NK cells participate to a higher cytokine response 24 h after infection by delivering IFN-γ to XCR1$^+$ DCs and monocytes to sustain the production of IL-12 and the expression of inducible nitric oxide synthase, respectively (Kang et al., 2008; Lee et al., 2013). Interestingly, the pattern of NK cell migration during secondary infection differs in terms of time and localization in the spleen as compared with primary infection. We found that, as soon as 6 h after secondary challenge, NK cells, mCTLs, and XCR1$^+$ DCs form clusters. These clusters localize at the edges of the marginal zone around B cell follicles in the RP through which the bacteria colonizes the spleen. The signals triggering the recruitment of NK cells into these clusters are not yet known but CXCR3 engagement was not necessary (unpublished data). NK cells express multiple chemokine receptors, including CCR2, CCR5, and CXCR3 (Mack et al., 2001; Bernardini et al., 2012). Hence, multiple chemokine receptors may exert redundant roles for NK cell recruitment into clusters of XCR1$^+$ DCs upon *Lm* secondary infection. How does the attraction of NK cells by XCR1$^+$ DCs influence the recall of mCTL responses? Here, we show that NK cells and XCR1$^+$ DCs interact in well-organized clusters in the RP early after secondary infection by *Lm* and that this process amplifies IFN-γ and IL-12 production by NK cells and XCR1$^+$ DCs, respectively, promoting the downstream activation of mCTLs. Several reports focused on primary immune responses have demonstrated that the effectiveness of NK cell activation influences CD8$^+$ T cell responses such as occurring during acute infections with mouse cytomegalovirus (Robbins et al., 2007; Mitrović et al., 2012), during chronic infections with LCMV (Whitmire et al., 2008), or in response to tumor engraftments (Adam et al., 2005). Altogether, these studies suggest that early interactions between DCs and NK cells contribute to orchestrate adaptive immunity against infections or tumors (Walzer et al., 2005), not only during acute primary immune responses but also in chronic infections or upon secondary challenges, by modulating the kinetic and intensity of CD4$^+$ and CD8$^+$ T cell responses depending on nature of the threat faced by the host.

CXCL9/CXCR3 signaling is implicated in the redistribution of central memory T cells in interfollicular area and subcapsular regions in LN near pathogen entry site upon viral infections (Sung et al., 2012; Kastenmüller et al., 2013). In these studies, CXCL9 was secreted by macrophages, monocytes, and CD11c$^+$ DCs, which reside in the outermost areas in LN, to be presented on stromal cells, and to provide a guidance signal allowing a zone to zone relocalization of central memory T cells. Our study extends this concept to the immune response against another type of pathogen, an intracellular bacterium, and in another organ, the spleen, by demonstrating that CXCR3 signaling contributes to the microanatomical relocation of splenic RP mCTLs around CXCL9-producing XCR1$^+$ DCs. Together with CXCL9, CXCL10 and CXCL11 are also high-affinity ligands for CXCR3. CXCL11 is not functional in *C57BL/6J* mice as a result of a single-point mutation within the coding sequence resulting in a frame shift (Carter et al., 2007). CXCL9 and CXCL10 expressions, which are strongly induced in spleen upon *Lm-OVA* secondary infection, were decreased in XCR1$^+$ DC-depleted mice (Fig. 7 D and not depicted). Therefore, CXCL9 and CXCL10 might play redundant roles in the attraction of mCTLs in our experimental settings. Altogether, these results strongly suggest that the engagement of CXCR3 on mCTLs by CXCL9 and CXCL10 produced by myeloid cells upon sensing of danger signals may be a general and critical mechanism orchestrating in time and space the recall of adaptive cellular immunity against secondary infections by intracellular pathogens or against tumor resurgence.

In conclusion, by using the *Karma* mouse model, we discovered that XCR1$^+$ DCs promote the reactivation of mCTLs upon *Lm*, VSV, and VV secondary infections. We defined some of the underlying cellular and molecular mechanisms leading to the early activation of mCTLs upon *Lm*

secondary *Lm-OVA* infection, cut in equal halves and processed either for flow cytometry or confocal imaging. Frequency of OT-I mCTLs (F) and of polyclonal CD44^{hi} mCTLs (G) that produce IFN-γ 6 h post-secondary infection was measured as in Fig. 3. (H) Spleen sections were stained with anti-B220 (dark blue) and anti-GFP (green), and analyzed by confocal microscopy. Bar, 500 µm. Arrows show clusters. One representative experiment of three, each with at least three mice per group, is shown. Graph represents percentage of OT-I mCTLs that form clusters in anti–CXCR3-treated memory mice as mathematically determined. Data (mean ± SEM) are pooled from two independent experiments, each including at least three mice per group. *, $P < 0.05$; **, $P < 0.01$.

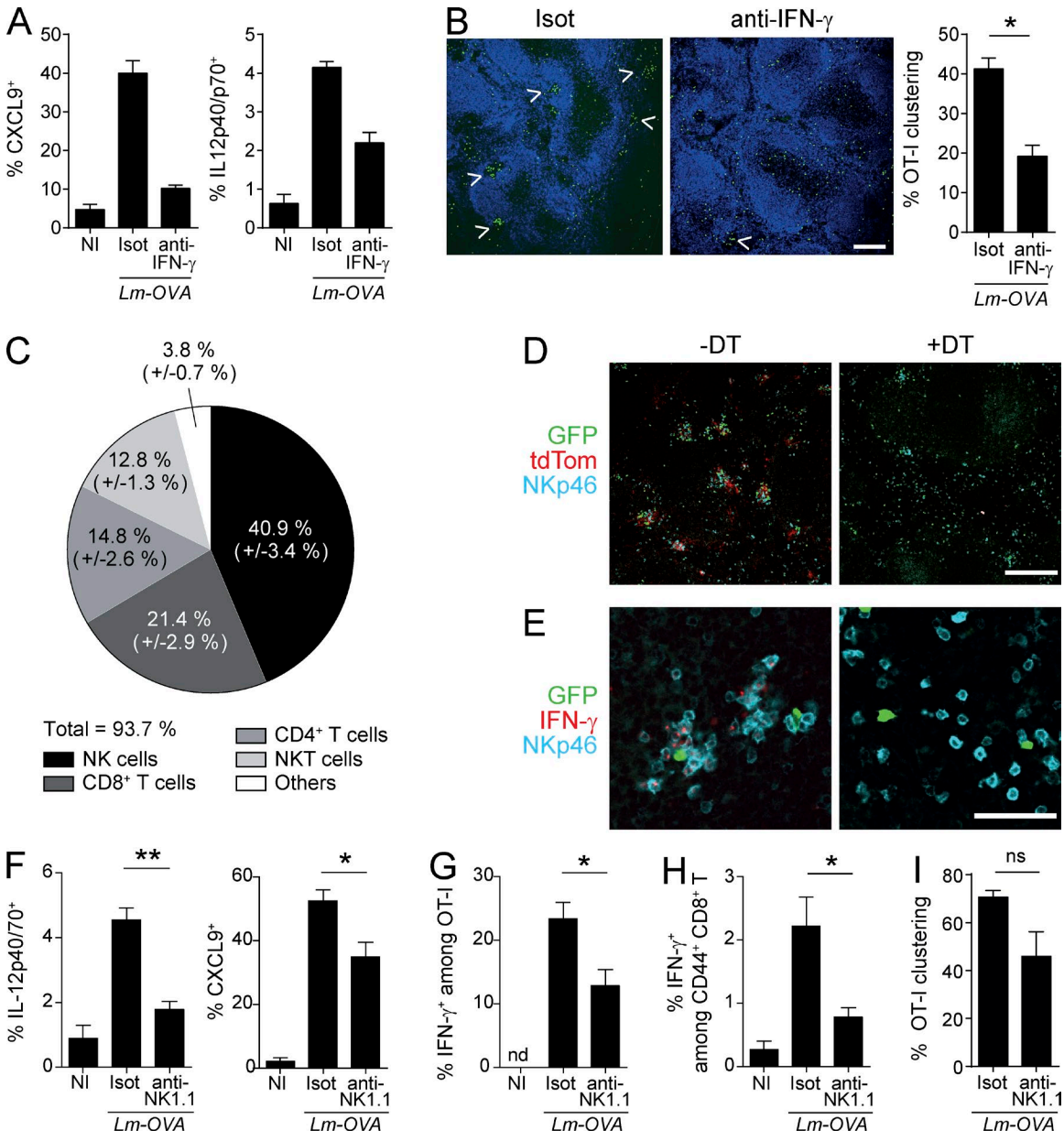

Figure 8. **The early IFN-γ production participates in the clustering of mCTLs after secondary infection.** IFN-γ–blocking antibodies (anti–IFN-γ) or isotype control (Isot) were injected to memory mice 18 h before secondary infection. Spleens were harvested at 6 h after, cut in equal halves, and processed either for flow cytometry or confocal imaging. (A) Frequency of IL-12p40/70 and CXCL9-producing XCR1$^+$ DCs in spleens. (B) Spleen sections were stained for GFP (green) and B220 (dark blue). Bar, 200 µm. Arrows show clusters. Graph represents percentage of OT-I mCTLs that form clusters in anti–IFN-γ–treated memory mice as mathematically determined. Data (mean ± SEM) are shown for one experiment representative of two independent ones, each with at least three mice per group. *, $P < 0.05$; ns, nonsignificant. (C) Spleens of memory mice were harvested 6 h after secondary infection. Circle diagram encompasses all cells that stained positive for IFN-γ. One representative experiment out of four with three mice per group is shown. (D and E) Spleens from memory mice were fixed 6 h after the infection, and sections were stained with anti-GFP (green), anti-dsRed (red), and anti-NKp46 (cyan; bar, 200 µm; D), or with anti-GFP (green), anti–IFN-γ (red) and anti-NKp46 (cyan; bar, 50 µm; E). One representative experiment out of two, each with three mice per group, is shown. (F-I) Impact of NK cell depletion. (F) Frequency of IL-12p40/70 and CXCL9-producing XCR1$^+$ DCs in spleens 6 h after *Lm-OVA* secondary infection. Data (mean ± SEM) are pooled from two independent experiments, each with at least three mice per group. *, $P < 0.05$; **, $P < 0.01$. (G and H) Frequency of OT-I mCTLs (G) and of polyclonal CD44^{hi} mCTLs (H) that produce IFN-γ 6 h post-secondary infection was measured as in Fig. 3. One experiment representative of three independent ones, each with five mice per group is shown. Data are represented as mean ± SEM. *, $P < 0.05$. (I) Statistical analysis of clustered OT-I mCTLs. Data (mean ± SEM) are pooled from two independent experiments, each with at least three mice per group.

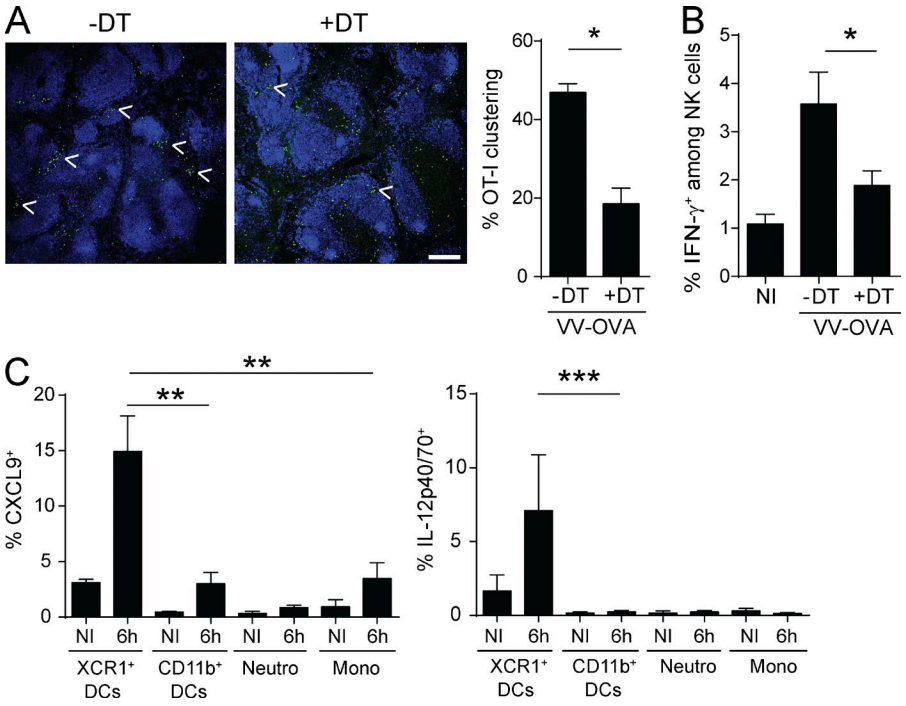

Figure 9. **XCR1⁺ DCs are the major producers of IL-12 and CXCL9, and promote mCTL clustering upon secondary infection with VV-OVA.** *Karma* mice received 500–1,000 naive GFP⁺ OT-I cells 1 d before primary infection with *Lm-OVA*. 30 d later, mice were treated with DT or left untreated, and secondary infected with VV-OVA. Spleens were harvested 6 h after secondary challenge. (A) Spleen sections from untreated or DT-treated memory *Karma* mice were stained with anti-B220 (dark blue) and anti-GFP (green), and analyzed by confocal microscopy. Bar, 200 µm. Statistical analysis of the frequency of OT-I mCTLs found clustered around the follicles. Graph shows data (mean ± SEM) from one representative of two independent experiments each with at least three mice per group. *, $P < 0.05$. (B) Analysis of IFN-γ induction in NK cells 6 h after VV-OVA secondary challenge. Splenocytes were harvested, incubated with brefeldin A before intracellular staining of IFN-γ. Data (mean ± SEM) are shown from one representative of two independent experiments, each with at least three mice per group. *, $P < 0.05$. (C) The induction of IL-12p40/70 and CXCL9 was analyzed by flow cytometry in several splenocyte populations (see Fig. S3 for the detailed gating of cells). Intracellular staining was performed directly ex vivo without prior incubation with brefeldin A. Data (mean ± SEM) shown are pooled from two independent experiments, each with at least three mice per group. **, $P < 0.01$; ***, $P < 0.001$.

infection. This study revealed that, besides their classical function as professional antigen cross-presenting cells critical for the priming of naive CD8⁺ T cells against many intracellular pathogens and against tumors, XCR1⁺ DCs are also endowed with immunoregulatory functions, such as IL-12 and CXCL9 production, which contribute to orchestrate in time and space the reactivation of mCTLs.

MATERIALS AND METHODS

Ethics statement regarding care and use of animals for experimentation. The animal care and use protocols (authorization ID no. 11–09/09/2011) were designed in accordance with national and international laws for laboratory animal welfare and experimentation (EEC Council Directive 2010/63/EU, September 2010), and approved by the Marseille Ethical Committee for Animal Experimentation (registered by the Comité National de Réflexion Ethique sur l'Expérimentation Animale under no. 14).

Mice and in vivo treatments. The *Karma* mice (*a530099j19rik*^{tm1Ciphe}) were made according to a standard gene targeting approach in *C57BL/6N*-derived ES cells. They were constructed by inserting the *IRES-tdTomato-2A-hDTR* cassette into the 3′-UTR of *a530099j19rik* gene. *Karma* mice were outcrossed for three generations with WT *C57BL/6J* mice, and *Karma* littermates were used as DT-untreated controls. For neutralizing antibody experiments, WT *C57BL/6J* mice were purchased from Charles River Laboratories. *Tg*^{TcraTcrb1100Mjb}*; Rag1*$^{-/-}$*; Rag2*$^{-/-}$ (OT-I) mice (gift from A.-M. Schmidt-Verhulst, Centre d'Immunologie de Marseille-Luminy [CIML], Marseille, France) were bred with *C57BL/6 ubiquitinC-GFP* mice (C57BL/6-Tg(UBC-GFP)30Scha/J; gift from Marc Bajénoff, CIML, Marseille, France) to obtain *Tg*^{TcraTcrb1100Mjb}*; Rag2*$^{-/-}$*; Ubc-GFP*$^{+/+}$ mice, from which we routinely isolated GFP-expressing OT-I cells. For complete XCR1⁺ DC depletion, a dose of 32 ng/g of body weight of DT (Merck) was administrated at least 6 h before the experiment. For sustained depletion, mice were first injected with 32 ng/g of DT, then received one injection of 16 ng/g every 60 h. This was efficient to deplete XCR1⁺ DCs for at least 10 d. DT was diluted in cold endotoxin free PBS. For in vivo antibody-dependent neutralization or antibody-mediated cell depletion, *Karma* memory mice were injected i.p. with purified antibodies or their corresponding isotypes (anti-NK1.1, 200 µg; anti-CXCR3, anti–IL-12, and anti–IFN-γ, 500 µg) 1 d before secondary infection. Antibodies are listed in Table S1.

Antigen cross-presentation assay and cytokine response to STAg. For cross-presentation assay, *Karma* mice received a single injection of DT or PBS (control) 1 d before i.v. injection of 2.5 mg of soluble OVA (Sigma-Aldrich). Splenic $CD11c^+$ cells from *Karma* mice were enriched to >95% purity using CD11c microbeads (Miltenyi Biotec). Splenic OT-I cells were purified with Dynal mouse CD8 cell negative isolation kit (Invitrogen), and labeled with CFSE. $CD11c^+$ and OT-I cells were co-cultured for 3 d at different ratio in complete medium supplemented with IL-2. OT-I cell proliferation represented by CFSE dilution was assessed by flow cytometry, and absolute numbers of OT-I cells were determined using Flow-Count Fluorospheres (Beckman Coulter).

For cytokine response to STAg, *Karma* mice received a single injection of DT or PBS (control) 1d before i.v. injection of 6 μg of STAg (gift from G.S. Yap, Rutgers New Jersey Medical School, Newark, NJ). Sera were collected 12 h after to detect systemic IL-12p70 induction by ELISA (eBioscience).

Microbes. Unless stated otherwise in the figure legend, mice were immunized with the following OVA-expressing recombinant microbes: 5×10^3 colony-forming-units (CFU) of *Listeria-OVA* (*Lm-OVA*), 10^5 PFU of Vaccinia-OVA (VV-OVA) or 2×10^4 PFU of VSV-OVA (from T. Lawrence, CIML, Marseille, France). Memory mice were secondary challenged with 10^6 CFU of *Lm-OVA*, 2×10^6 PFU of VV-OVA or of VSV-OVA, and 3×10^4 PFU of MCMV-OVA (from E. Vivier, CIML, Marseille, France). Splenocytes were analyzed by flow cytometry 5 d later.

***Lm* infection and quantification of bacterial titers.** The 10403s strain, either WT *Lm* or *Lm-OVA*, was obtained from G. Lauvau (Albert Einstein College of Medicine, New York, NY). Frozen aliquots of *Lm* were grown in brain-heart infusion (BHI) medium to a logarithmic phase (OD600 = 0.05–0.17) and diluted in PBS before i.v. inoculation. After each infection, inocula were routinely plated on BHI agar plates to confirm their titers. For UV-C irradiation of *Lm-OVA*, fresh bacterium culture was washed twice in PBS. Suspension of 10^9–10^{10} bacteria/ml in PBS was exposed to an UVC lamp (254 nm; 5 J/cm^2) before being stained for 10 min at 37°C with 50 μM of CFSE. Lack of growth of UV-C–inactivated *Lm-OVA* was confirmed by culturing 2×10^9 bacteria for 48 h at 37°C on BHI agar. Mice were inoculated with freshly prepared 10^8 CFU of UV-C–irradiated CFSE-stained *Lm-OVA*. To measure bacterial titers, spleens were dissociated on nylon mesh in 0.2% NP-40 (Igepal CA630; Sigma-Aldrich). Serial dilutions were performed in the same buffer and were plated onto BHI agar plates. CFU numbers were counted at least 24 h later.

Spleen preparation and flow cytometry analysis. Cell suspensions from spleens and CLNs were prepared and stained as described previously (Crozat et al., 2011). The antibodies used for flow cytometry are listed in the Table S1. Stained cell acquisition was performed on a FACSCanto II, or on a LSR-II upgraded with a 561nm laser when detection of td-Tomato expression was required.

Analysis of memory $CD8^+$ T cell responses. 500–1,000 naive GFP-expressing OT-I cells were i.v. transferred in *Karma* mice 1 d before *Lm* primary infection. 30 d later, DT or neutralizing antibodies was administrated to the mice before secondary infection with *Lm-OVA*. When spleens and blood were harvested 5 d after secondary infections, cells were stained with H2-K^b SIINFEKL tetramers (Beckman Coulter) to identify OVA-specific $CD8^+$ T cells. Splenocytes were also incubated for 4 h with 1 μM of SIINFEKL and Brefeldin A to detect intracellular IFN-γ, CCL3, and Granzyme B. When spleens were harvested 6 h after secondary infection, splenocytes were incubated for 3 h with Brefeldin A in complete RPMI medium to detect spontaneous IFN-γ production in lymphocytes.

Immunofluorescence. Spleens were harvested, cut in 5-mm pieces, and fixed for at least 1 h in Antigenfix (DiaPath), then washed in phosphate buffer (PB1X: 0.02 M NaH_2PO_4 and 0.08 M Na_2HPO_4) for 1 h, dehydrated in 30% sucrose overnight at 4°C, and embedded in OCT freezing media (Sakura Fineteck). 16-μm frozen sections of spleens were blocked in PB1X containing 0.2% saponin, 2% BSA, and 2% 2.4G2 supernatant, and stained in PB1X, 0.2% saponin. When the staining required, further blocking steps with normal goat or rabbit sera were added. Stained sections were mounted in ProLong Gold antifade reagent (Invitrogen), and acquired on a LSM780 confocal microscope (Carl Zeiss). TdTomato expression was amplified by using an anti-Red Fluorescent Protein (RFP) antibody (Rockland). Antibodies used in immunofluorescence are detailed in Table S1.

Quantification of memory OT-I cell clustering and migration into the T cell zone. OT-I cell clustering and migration into T cell zones were determined computationally using ImageJ and R graphical user interface (GUI) software. We used mosaic images representing a complete section of spleen to perform this analysis. For OT-I cell clustering: a macro program developed for Image J allowed us to spot individual GFP^+ OT-I cells present on a frozen spleen section. When several GFP^+ OT-I cells were too close to be detected as individual cells by the macro program due to strong signal intensity, we manually separated them using the pencil tool from ImageJ. Coordinates of each distinct GFP^+ OT-I cell were retrieved. OT-I cell locations were then represented graphically with R software after installing the Fixed Point Cluster (FPC) analysis package. The DBSCAN algorithm was set to define a true cluster as a group of three or more proximate cells. Percent of clustered cells were then calculated according to the total number of cells present on the whole section. For OT-I localization in the T cell zone: a macro program developed for Image J allowed us to enumerate all individual GFP^+ OT-I

cells, as well as GFP$^+$ OT-I cells found in T cell zones. As previously, merged GFP$^+$ OT-I cells were manually separated. T cell regions were manually delimited according to B220 staining of B cell follicles and nuclear density.

Microarray data. The data were downloaded from the BioGPS public database (http://biogps.gnf.org; Gene Expression Omnibus dataset number GSE10246).

Statistical analyses. Statistical analyses were performed using nonparametric Mann-Whitney tests in all experiments.

Online supplemental material. Table S1 lists the antibodies used in this study. Fig. S1 shows the gating strategy used to identify DC subsets in spleen, skin, and CLNs. Fig. S2 shows the gating strategy used to analyze tetramer-positive mCTLs and the early activation of mCTLs in secondary infected animals. Fig. S3 shows IL-12 and CXCL9 expression analysis on DCs, neutrophils and monocytes from secondary infected animals. Fig. S4 shows a schematic model of the recall of mCTLs by XCR1$^+$ DCs during secondary *Lm* infection. Online supplemental material is available at http://www.jem.org/cgi/content/full/jem.20142350/DC1.

ACKNOWLEDGMENTS

We thank Bruno Estebe, Frédéric Fiore, and Bernard Malissen (Centre d'Immunophénomique [CIPHE], UM2 Aix-Marseille Université, Institut National de la Santé et de la Recherche Médicale US012, Centre National de la Recherche Scientifique UMS3367, Marseille, France) for generating the *Karma* mice; Marilyn Boyron, and the cytometry and ImagImm core facilities (CIML, UMR7280, France) for technical assistance; Mathieu Fallet (CIML, UMR7280, France) for programming macros to quantify memory OT-I cell clustering and migration into the T cell zone; and Toby Lawrence and Elena Tomasello for critical reading of the manuscript. We acknowledge France-BioImaging infrastructure supported by the Agence Nationale de la Recherche (ANR-10-INSB-04-01, call "Investissements d'Avenir").

This work was supported by institutional funding from CNRS and Inserm, by the Innate Immunocytes in Health and Disease (I2HD) collaborative project between CIML, AVIESAN, and SANOFI, and by grants from Association pour la recherche sur le cancer (ARC), from Fondation pour la Recherche Médicale (label "Equipe FRM 2011", project number DEQ20110421284) and from the European Research Council under the European Community's Seventh Framework Program (FP7/2007–2013 grant agreement number 281225). Y.O. Alexandre was supported by doctoral fellowships from the French Ministère de l'Enseignement Supérieur et de la Recherche, and from ARC. S. Ghilas was laureate from a "University President" Excellence Ph.D. Fellowship from Aix Marseille Université and from ARC. C. Sanchez was supported by the I2HD CIML-SANOFI project.

The authors declare no competing financial interests.

Submitted: 17 December 2014

Accepted: 20 November 2015

REFERENCES

Adam, C., S. King, T. Allgeier, H. Braumüller, C. Lüking, J. Mysliwietz, A. Kriegeskorte, D.H. Busch, M. Röcken, and R. Mocikat. 2005. DC-NK cell cross talk as a novel CD4$^+$ T-cell-independent pathway for antitumor CTL induction. *Blood.* 106:338–344. http://dx.doi.org/10.1182/blood-2004-09-3775

Aoshi, T., B.H. Zinselmeyer, V. Konjufca, J.N. Lynch, X. Zhang, Y. Koide, and M.J. Miller. 2008. Bacterial entry to the splenic white pulp initiates antigen presentation to CD8$^+$ T cells. *Immunity.* 29:476–486. http://dx.doi.org/10.1016/j.immuni.2008.06.013

Bajénoff, M., E. Narni-Mancinelli, F. Brau, and G. Lauvau. 2010. Visualizing early splenic memory CD8$^+$ T cells reactivation against intracellular bacteria in the mouse. *PLoS One.* 5:e11524. http://dx.doi.org/10.1371/journal.pone.0011524

Bar-On, L., and S. Jung. 2010a. Defining dendritic cells by conditional and constitutive cell ablation. *Immunol. Rev.* 234:76–89. http://dx.doi.org/10.1111/j.0105-2896.2009.00875.x

Bar-On, L., and S. Jung. 2010b. Defining in vivo dendritic cell functions using CD11c-DTR transgenic mice. *Methods Mol. Biol.* 595:429–442. http://dx.doi.org/10.1007/978-1-60761-421-0_28

Belz, G.T., S. Bedoui, F. Kupresanin, F.R. Carbone, and W.R. Heath. 2007. Minimal activation of memory CD8$^+$ T cell by tissue-derived dendritic cells favors the stimulation of naive CD8$^+$ T cells. *Nat. Immunol.* 8:1060–1066. http://dx.doi.org/10.1038/ni1505

Berg, R.E., E. Crossley, S. Murray, and J. Forman. 2003. Memory CD8$^+$ T cells provide innate immune protection against *Listeria monocytogenes* in the absence of cognate antigen. *J. Exp. Med.* 198:1583–1593. http://dx.doi.org/10.1084/jem.20031051

Bernardini, G., A. Gismondi, and A. Santoni. 2012. Chemokines and NK cells: regulators of development, trafficking and functions. *Immunol. Lett.* 145:39–46. http://dx.doi.org/10.1016/j.imlet.2012.04.014

Broz, M.L., M. Binnewies, B. Boldajipour, A.E. Nelson, J.L. Pollack, D.J. Erle, A. Barczak, M.D. Rosenblum, A. Daud, D.L. Barber, et al. 2014. Dissecting the tumor myeloid compartment reveals rare activating antigen-presenting cells critical for T cell immunity. *Cancer Cell.* 26:638–652. http://dx.doi.org/10.1016/j.ccell.2014.09.007

Campisi, L., S.M. Soudja, J. Cazareth, D. Bassand, A. Lazzari, F. Brau, E. Narni-Mancinelli, N. Glaichenhaus, F. Geissmann, and G. Lauvau. 2011. Splenic CD8α$^+$ dendritic cells undergo rapid programming by cytosolic bacteria and inflammation to induce protective CD8$^+$ T-cell memory. *Eur. J. Immunol.* 41:1594–1605. http://dx.doi.org/10.1002/eji.201041036

Carter, S.L., M. Müller, P.M. Manders, and I.L. Campbell. 2007. Induction of the genes for Cxcl9 and Cxcl10 is dependent on IFN-gamma but shows differential cellular expression in experimental autoimmune encephalomyelitis and by astrocytes and microglia in vitro. *Glia.* 55:1728–1739. http://dx.doi.org/10.1002/glia.20587

Croft, M., L.M. Bradley, and S.L. Swain. 1994. Naive versus memory CD4 T cell response to antigen. Memory cells are less dependent on accessory cell costimulation and can respond to many antigen-presenting cell types including resting B cells. *J. Immunol.* 152:2675–2685.

Crozat, K., S. Tamoutounour, T.P. Vu Manh, E. Fossum, H. Luche, L. Ardouin, M. Guilliams, H. Azukizawa, B. Bogen, B. Malissen, et al. 2011. Cutting edge: expression of XCR1 defines mouse lymphoid-tissue resident and migratory dendritic cells of the CD8α$^+$ type. *J. Immunol.* 187:4411–4415. http://dx.doi.org/10.4049/jimmunol.1101717

Curtsinger, J.M., D.C. Lins, and M.F. Mescher. 1998. CD8+ memory T cells (CD44^{high}, Ly-6C$^+$) are more sensitive than naive cells to (CD44low, Ly-6C-) to TCR/CD8 signaling in response to antigen. *J. Immunol.* 160:3236–3243.

Dengler, T.J., and J.S. Pober. 2000. Human vascular endothelial cells stimulate memory but not naive CD8$^+$ T cells to differentiate into CTL retaining an early activation phenotype. *J. Immunol.* 164:5146–5155. http://dx.doi.org/10.4049/jimmunol.164.10.5146

Dutertre, C.A., L.F. Wang, and F. Ginhoux. 2014. Aligning bona fide dendritic cell populations across species. *Cell. Immunol.* 291:3–10. http://dx.doi.org/10.1016/j.cellimm.2014.08.006

Edelson, B.T., T.R. Bradstreet, K. Hildner, J.A. Carrero, K.E. Frederick, W. Kc, R. Belizaire, T. Aoshi, R.D. Schreiber, M.J. Miller, et al. 2011a. CD8α$^+$ dendritic cells are an obligate cellular entry point for productive infection by *Listeria monocytogenes*. *Immunity.* 35:236–248. http://dx.doi.org/10.1016/j.immuni.2011.06.012

Edelson, B.T., T.R. Bradstreet, W. Kc, K. Hildner, J.W. Herzog, J. Sim, J.H. Russell, T.L. Murphy, E.R. Unanue, and K.M. Murphy. 2011b. Batf3-dependent CD11b(low/-) peripheral dendritic cells are GM-CSF-independent and are not required for Th cell priming after subcutaneous immunization. *PLoS One.* 6:e25660. http://dx.doi.org/10.1371/journal.pone.0025660

Eickhoff, S., A. Brewitz, M.Y. Gerner, F. Klauschen, K. Komander, H. Hemmi, N. Garbi, T. Kaisho, R.N. Germain, and W. Kastenmüller. 2015. Robust anti-viral immunity requires multiple distinct T cell-dendritic cell interactions. *Cell.* 162:1322–1337. http://dx.doi.org/10.1016/j.cell.2015.08.004

Elpek, K.G., A. Bellemare-Pelletier, D. Malhotra, E.D. Reynoso, V. Lukacs-Kornek, R.H. DeKruyff, and S.J. Turley. 2011. Lymphoid organ-resident dendritic cells exhibit unique transcriptional fingerprints based on subset and site. *PLoS One.* 6:e23921. http://dx.doi.org/10.1371/journal.pone.0023921

Farber, D.L. 2009. Biochemical signaling pathways for memory T cell recall. *Semin. Immunol.* 21:84–91. http://dx.doi.org/10.1016/j.smim.2009.02.003

Fukaya, T., R. Murakami, H. Takagi, K. Sato, Y. Sato, H. Otsuka, M. Ohno, A. Hijikata, O. Ohara, M. Hikida, et al. 2012. Conditional ablation of CD205$^+$ conventional dendritic cells impacts the regulation of T-cell immunity and homeostasis in vivo. *Proc. Natl. Acad. Sci. USA.* 109:11288–11293. http://dx.doi.org/10.1073/pnas.1202208109

Heng, T.S., and M.W. Painter. Immunological Genome Project Consortium. 2008. The Immunological Genome Project: networks of gene expression in immune cells. *Nat. Immunol.* 9:1091–1094. http://dx.doi.org/10.1038/ni1008-1091

Hor, J.L., P.G. Whitney, A. Zaid, A.G. Brooks, W.R. Heath, and S.N. Mueller. 2015. Spatiotemporally distinct interactions with dendritic cell subsets facilitates CD4$^+$ and CD8$^+$ T cell activation to localized viral infection. *Immunity.* 43:554–565. http://dx.doi.org/10.1016/j.immuni.2015.07.020

Jiang, W., W.J. Swiggard, C. Heufler, M. Peng, A. Mirza, R.M. Steinman, and M.C. Nussenzweig. 1995. The receptor DEC-205 expressed by dendritic cells and thymic epithelial cells is involved in antigen processing. *Nature.* 375:151–155. http://dx.doi.org/10.1038/375151a0

Kang, S.J., H.E. Liang, B. Reizis, and R.M. Locksley. 2008. Regulation of hierarchical clustering and activation of innate immune cells by dendritic cells. *Immunity.* 29:819–833. http://dx.doi.org/10.1016/j.immuni.2008.09.017

Kastenmüller, W., M. Brandes, Z. Wang, J. Herz, J.G. Egen, and R.N. Germain. 2013. Peripheral prepositioning and local CXCL9 chemokine-mediated guidance orchestrate rapid memory CD8$^+$ T cell responses in the lymph node. *Immunity.* 38:502–513. http://dx.doi.org/10.1016/j.immuni.2012.11.012

Kissenpfennig, A., S. Henri, B. Dubois, C. Laplace-Builhé, P. Perrin, N. Romani, C.H. Tripp, P. Douillard, L. Leserman, D. Kaiserlian, et al. 2005. Dynamics and function of Langerhans cells in vivo: dermal dendritic cells colonize lymph node areas distinct from slower migrating Langerhans cells. *Immunity.* 22:643–654. http://dx.doi.org/10.1016/j.immuni.2005.04.004

Kumar, R., M. Ferez, M. Swamy, I. Arechaga, M.T. Rejas, J.M. Valpuesta, W.W. Schamel, B. Alarcon, and H.M. van Santen. 2011. Increased sensitivity of antigen-experienced T cells through the enrichment of oligomeric T cell receptor complexes. *Immunity.* 35:375–387. http://dx.doi.org/10.1016/j.immuni.2011.08.010

Lee, S.H., J.A. Carrero, R. Uppaluri, J.M. White, J.M. Archambault, K.S. Lai, S.R. Chan, K.C. Sheehan, E.R. Unanue, and R.D. Schreiber. 2013. Identifying the initiating events of anti-Listeria responses using mice with conditional loss of IFN-γ receptor subunit 1 (IFNGR1). *J. Immunol.* 191:4223–4234. http://dx.doi.org/10.4049/jimmunol.1300910

London, C.A., M.P. Lodge, and A.K. Abbas. 2000. Functional responses and costimulator dependence of memory CD4$^+$ T cells. *J. Immunol.* 164:265–272. http://dx.doi.org/10.4049/jimmunol.164.1.265

Mack, M., J. Cihak, C. Simonis, B. Luckow, A.E. Proudfoot, J. Plachý, H. Brühl, M. Frink, H.J. Anders, V. Vielhauer, et al. 2001. Expression and characterization of the chemokine receptors CCR2 and CCR5 in mice. *J. Immunol.* 166:4697–4704. http://dx.doi.org/10.4049/jimmunol.166.7.4697

Macleod, B.L., S. Bedoui, J.L. Hor, S.N. Mueller, T.A. Russell, N.A. Hollett, W.R. Heath, D.C. Tscharke, A.G. Brooks, and T. Gebhardt. 2014. Distinct APC subtypes drive spatially segregated CD4$^+$ and CD8$^+$ T-cell effector activity during skin infection with HSV-1. *PLoS Pathog.* 10:e1004303. http://dx.doi.org/10.1371/journal.ppat.1004303

Mehlhop-Williams, E.R., and M.J. Bevan. 2014. Memory CD8$^+$ T cells exhibit increased antigen threshold requirements for recall proliferation. *J. Exp. Med.* 211:345–356. http://dx.doi.org/10.1084/jem.20131271

Miller, J.C., B.D. Brown, T. Shay, E.L. Gautier, V. Jojic, A. Cohain, G. Pandey, M. Leboeuf, K.G. Elpek, J. Helft, et al. Immunological Genome Consortium. 2012. Deciphering the transcriptional network of the dendritic cell lineage. *Nat. Immunol.* 13:888–899. http://dx.doi.org/10.1038/ni.2370

Mitrović, M., J. Arapović, L. Traven, A. Krmpotić, and S. Jonjić. 2012. Innate immunity regulates adaptive immune response: lessons learned from studying the interplay between NK and CD8$^+$ T cells during MCMV infection. *Med. Microbiol. Immunol. (Berl.).* 201:487–495. http://dx.doi.org/10.1007/s00430-012-0263-0

Mott, K.R., H. Maazi, S.J. Allen, M. Zandian, H. Matundan, Y.N. Ghiasi, B.G. Sharifi, D. Underhill, O. Akbari, and H. Ghiasi. 2015. Batf3 deficiency is not critical for the generation of CD8α$^+$ dendritic cells. *Immunobiology.* 220:518–524. http://dx.doi.org/10.1016/j.imbio.2014.10.019

Muraille, E., R. Giannino, P. Guirnalda, I. Leiner, S. Jung, E.G. Pamer, and G. Lauvau. 2005. Distinct in vivo dendritic cell activation by live versus killed *Listeria monocytogenes*. *Eur. J. Immunol.* 35:1463–1471. http://dx.doi.org/10.1002/eji.200526024

Muraille, E., E. Narni-Mancinelli, P. Gounon, D. Bassand, N. Glaichenhaus, L.L. Lenz, and G. Lauvau. 2007. Cytosolic expression of SecA2 is a prerequisite for long-term protective immunity. *Cell. Microbiol.* 9:1445–1454. http://dx.doi.org/10.1111/j.1462-5822.2007.00883.x

Neuenhahn, M., K.M. Kerksiek, M. Nauerth, M.H. Suhre, M. Schiemann, F.E. Gebhardt, C. Stemberger, K. Panthel, S. Schröder, T. Chakraborty, et al. 2006. CD8α$^+$ dendritic cells are required for efficient entry of *Listeria monocytogenes* into the spleen. *Immunity.* 25:619–630. http://dx.doi.org/10.1016/j.immuni.2006.07.017

Obar, J.J., K.M. Khanna, and L. Lefrançois. 2008. Endogenous naive CD8+ T cell precursor frequency regulates primary and memory responses to infection. *Immunity.* 28:859–869. http://dx.doi.org/10.1016/j.immuni.2008.04.010

Pihlgren, M., P.M. Dubois, M. Tomkowiak, T. Sjögren, and J. Marvel. 1996. Resting memory CD8+ T cells are hyperreactive to antigenic challenge in vitro. *J. Exp. Med.* 184:2141–2151. http://dx.doi.org/10.1084/jem.184.6.2141

Piva, L., P. Tetlak, C. Claser, K. Karjalainen, L. Renia, and C. Ruedl. 2012. Cutting edge: Clec9A+ dendritic cells mediate the development of experimental cerebral malaria. *J. Immunol.* 189:1128–1132. http://dx.doi.org/10.4049/jimmunol.1201171

Probst, H.C., K. Tschannen, B. Odermatt, R. Schwendener, R.M. Zinkernagel, and M. Van Den Broek. 2005. Histological analysis of CD11c-DTR/GFP mice after in vivo depletion of dendritic cells. *Clin. Exp. Immunol.* 141:398–404. http://dx.doi.org/10.1111/j.1365-2249.2005.02868.x

Qin, S., J.B. Rottman, P. Myers, N. Kassam, M. Weinblatt, M. Loetscher, A.E. Koch, B. Moser, and C.R. Mackay. 1998. The chemokine receptors CXCR3 and CCR5 mark subsets of T cells associated with certain inflammatory reactions. *J. Clin. Invest.* 101:746–754. http://dx.doi.org/10.1172/JCI1422

Rabin, R.L., M.K. Park, F. Liao, R. Swofford, D. Stephany, and J.M. Farber. 1999. Chemokine receptor responses on T cells are achieved through regulation of both receptor expression and signaling. *J. Immunol.* 162:3840–3850.

Richer, M.J., L.L. Pewe, L.S. Hancox, S.M. Hartwig, S.M. Varga, and J.T. Harty. 2015. Inflammatory IL-15 is required for optimal memory T cell responses. *J. Clin. Invest.* 125:3477–3490. http://dx.doi.org/10.1172/JCI81261

Robbins, S.H., G. Bessou, A. Cornillon, N. Zucchini, B. Rupp, Z. Ruzsics, T. Sacher, E. Tomasello, E. Vivier, U.H. Koszinowski, and M. Dalod. 2007. Natural killer cells promote early CD8 T cell responses against cytomegalovirus. *PLoS Pathog.* 3:e123. http://dx.doi.org/10.1371/journal.ppat.0030123

Robbins, S.H., T. Walzer, D. Dembélé, C. Thibault, A. Defays, G. Bessou, H. Xu, E. Vivier, M. Sellars, P. Pierre, et al. 2008. Novel insights into the relationships between dendritic cell subsets in human and mouse revealed by genome-wide expression profiling. *Genome Biol.* 9:R17. http://dx.doi.org/10.1186/gb-2008-9-1-r17

Rogers, P.R., C. Dubey, and S.L. Swain. 2000. Qualitative changes accompany memory T cell generation: faster, more effective responses at lower doses of antigen. *J. Immunol.* 164:2338–2346. http://dx.doi.org/10.4049/jimmunol.164.5.2338

Sancho, D., D. Mourão-Sá, O.P. Joffre, O. Schulz, N.C. Rogers, D.J. Pennington, J.R. Carlyle, and C. Reis e Sousa. 2008. Tumor therapy in mice via antigen targeting to a novel, DC-restricted C-type lectin. *J. Clin. Invest.* 118:2098–2110. http://dx.doi.org/10.1172/JCI34584

Schraml, B.U., J. van Blijswijk, S. Zelenay, P.G. Whitney, A. Filby, S.E. Acton, N.C. Rogers, N. Moncaut, J.J. Carvajal, and C. Reis e Sousa. 2013. Genetic tracing via DNGR-1 expression history defines dendritic cells as a hematopoietic lineage. *Cell.* 154:843–858. http://dx.doi.org/10.1016/j.cell.2013.07.014

Seillet, C., and G.T. Belz. 2013. Terminal differentiation of dendritic cells. *Adv. Immunol.* 120:185–210. http://dx.doi.org/10.1016/B978-0-12-417028-5.00007-7

Seillet, C., J.T. Jackson, K.A. Markey, H.J. Brady, G.R. Hill, K.P. Macdonald, S.L. Nutt, and G.T. Belz. 2013. CD8α^+ DCs can be induced in the absence of transcription factors Id2, Nfil3, and Batf3. *Blood.* 121:1574–1583. http://dx.doi.org/10.1182/blood-2012-07-445650

Shi, C., T.M. Hohl, I. Leiner, M.J. Equinda, X. Fan, and E.G. Pamer. 2011. Ly6G$^+$ neutrophils are dispensable for defense against systemic *Listeria monocytogenes* infection. *J. Immunol.* 187:5293–5298. http://dx.doi.org/10.4049/jimmunol.1101721

Soudja, S.M., A.L. Ruiz, J.C. Marie, and G. Lauvau. 2012. Inflammatory monocytes activate memory CD8$^+$ T and innate NK lymphocytes independent of cognate antigen during microbial pathogen invasion. *Immunity.* 37:549–562. http://dx.doi.org/10.1016/j.immuni.2012.05.029

Sung, J.H., H. Zhang, E.A. Moseman, D. Alvarez, M. Iannacone, S.E. Henrickson, J.C. de la Torre, J.R. Groom, A.D. Luster, and U.H. von Andrian. 2012. Chemokine guidance of central memory T cells is critical for antiviral recall responses in lymph nodes. *Cell.* 150:1249–1263. http://dx.doi.org/10.1016/j.cell.2012.08.015

van Helden, M.J., D.M. Zaiss, and A.J. Sijts. 2012. CCR2 defines a distinct population of NK cells and mediates their migration during influenza virus infection in mice. *PLoS One.* 7:e52027. http://dx.doi.org/10.1371/journal.pone.0052027

Vu Manh, T.P., N. Bertho, A. Hosmalin, I. Schwartz-Cornil, and M. Dalod. 2015a. Investigating evolutionary conservation of dendritic cell subset identity and functions. *Front. Immunol.* 6:260. http://dx.doi.org/10.3389/fimmu.2015.00260

Vu Manh, T.P., J. Elhmouzi-Younes, C. Urien, S. Ruscanu, L. Jouneau, M. Bourge, M. Moroldo, G. Foucras, H. Salmon, H. Marty, et al. 2015b. Defining mononuclear phagocyte subset homology across several distant warm-blooded vertebrates through comparative transcriptomics. *Front. Immunol.* 6:299. http://dx.doi.org/10.3389/fimmu.2015.00299

Walzer, T., M. Dalod, S.H. Robbins, L. Zitvogel, and E. Vivier. 2005. Natural-killer cells and dendritic cells: "l'union fait la force". *Blood.* 106:2252–2258. http://dx.doi.org/10.1182/blood-2005-03-1154

Whitmire, J.K., B. Eam, and J.L. Whitton. 2008. Tentative T cells: memory cells are quick to respond, but slow to divide. *PLoS Pathog.* 4:e1000041. http://dx.doi.org/10.1371/journal.ppat.1000041

Yamazaki, C., M. Sugiyama, T. Ohta, H. Hemmi, E. Hamada, I. Sasaki, Y. Fukuda, T. Yano, M. Nobuoka, T. Hirashima, et al. 2013. Critical roles of a dendritic cell subset expressing a chemokine receptor, XCR1. *J. Immunol.* 190:6071–6082. http://dx.doi.org/10.4049/jimmunol.1202798

Yarovinsky, F., D. Zhang, J.F. Andersen, G.L. Bannenberg, C.N. Serhan, M.S. Hayden, S. Hieny, F.S. Sutterwala, R.A. Flavell, S. Ghosh, and A. Sher. 2005. TLR11 activation of dendritic cells by a protozoan profilin-like protein. *Science.* 308:1626–1629. http://dx.doi.org/10.1126/science.1109893

Zammit, D.J., L.S. Cauley, Q.M. Pham, and L. Lefrançois. 2005. Dendritic cells maximize the memory CD8 T cell response to infection. *Immunity.* 22:561–570. http://dx.doi.org/10.1016/j.immuni.2005.03.005